Multi-view Three-Dimensional Fusion Echocardiography Using a Novel Respiratory Tracking Technique: First Results in Humans

by

Tyler Stanton Lamb

A thesis submitted in partial fulfillment of the requirements for the degree of

Master of Science

in

Translational Medicine

Department of Medicine

University of Alberta

Abstract

Introduction: 3-dimensional echocardiography (3DE) is currently the echocardiographic method of choice for quantification of left ventricular systolic function according to the American Society of Echocardiography. However, while developments in ultrasound transducer technology and post-processing techniques have undoubtedly bettered 3DE, they have failed to address inherent weaknesses of 3DE stemming from the nature of ultrasound physics. These include a limited field-of-view (FOV), reduced spatial and temporal resolution and reduced endocardial border definition (EBD) as compared to 2-dimensional echocardiography (2DE). In the context of echocardiography in general, poor EBD is largely explained by weakly reflected signals from important interfaces like the left ventricular (LV) endocardial border that often result from non-perpendicular angles of insonation. A technique called 'multi-view 3D fusion echocardiography' (M3DFE) provides a solution to this dilemma by fusing 3DE datasets from various complementary acoustic windows.

The thesis begins with a review of the literature around M3DFE and related topics. M3DFE has been previously studied in pre-clinical settings and has demonstrated favorable results by a number of investigators. Considering the existing literature, it is reasonable to infer that the most promising approach to M3DFE involves an optical tracking technique. Here, spatial alignment of datasets is accomplished through the optical tracking of both chest and transducer markers. However, two main challenges have not been adequately

addressed: i) no clinically feasible alignment protocol exists, and ii) there is no consensus on the optimal way to process overlapping portions of M3DFE datasets.

This thesis examines two hypotheses which, if proven true, have the potential to improve the feasibility and effectiveness of M3DFE and bring it closer to readiness for clinical testing. First, we hypothesize that a novel respiratory tracking technique based on quantitative optical tracking of chest markers can optimize alignment of datasets such that >90% will be suitable for diagnostic assessment as validated by an absence of perceptible misalignment. Second, we hypothesize that a fusion technique based on wavelet decomposition is superior to a more basic technique based on voxel averaging.

Methods: 3D Real-time M3DFE datasets were acquired from eleven volunteers during a breath-hold maneuver with three imaging protocols: i) using an unmoving transducer capturing a standard apical view, ii) using slight movements of the transducer to include non-standard apical views, and iii) with the transducer positioned at both apical and parasternal windows. Infrared cameras were used to track the 3D position and orientation of the transducer and chest markers. Chest marker tracking data was used to perform a novel quantitative screening procedure aimed at predicting adequate alignment of datasets. Multi-planar reconstruction of both M3DFE and standard apical 3DE datasets was performed to generate four- and two- chamber 2-dimensional planes which were then subjected to both fusion by voxel averaging and wavelet decomposition and compared. Subjective assessments included i) successful alignment of datasets and ii) EBD. Objective assessments included i) contrast, ii) contrast-to-noise ratio, iii) signal-to-noise ratio and iv) % increase in FOV.

Results: The quantitative screening procedure was effective and yielded a 97% rate of accurately predicting subjective alignment. Both fusion by voxel averaging and wavelet

decomposition improved subjective and objective measures of image quality and FOV. Wavelet decomposition was generally superior to voxel averaging with respect to contrast and EBD in all three imaging protocols, and with respect to SNR in the apical-parasternal protocol.

Conclusion: Our novel screening procedure based on quantitative optical tracking of chest markers is effective at optimizing alignment of M3DFE datasets. Results were generally supportive of the hypothesis that fusion by wavelet decomposition is a superior method to fusion by voxel averaging.

Preface

This thesis is an original work by Tyler Lamb and functions to fulfill part of the requirements for the degree, Master of Science in Translational Medicine. 100% of the writing was completed by Tyler Lamb. It should be noted, however, that this *project* was conducted in collaboration with the department of Computer Science at the University of Alberta (Dr. Pierre Boulanger, Dr. Kumaradevan Punithakumar and Dr. Abhilash Hareendranathan), a biostatistician (Dr. Wanhua Su at Grant MacEwan University), our research sonographer (Marina Choy), and under the guidance of my supervisor and mentor, Dr. Harald Becher.

Please note that this thesis follows a 'publication-based' format in accordance with formatting instructions provide by the Department of Medicine and Dr. Sean McMurty. Chapter 1 will be submitted for publication as a review article. Chapter 2 will be submitted for publication as an original research manuscript. Some descriptions and content are therefore redundant between these two chapters as they are written as stand-alone manuscripts. Chapter 3, which is entitled, "Future Directions and Conclusions" will not be published – it will function to provide a brief closing commentary on the project as a whole.

The research project, of which this thesis is a part, received research ethics approval from the University of Alberta Research Ethics Board, Project Name "Electromagnetic Tracking in Multiview 3D Fusion Echocardiography", Principal Investigator: Dr. Harald Becher, Study ID: Pro00057214, re-approved July 27, 2017, expires July 26, 2018.

Acknowledgments

I want to sincerely thank Dr. Choy and Dr. Shanks for their willingness to participate as members of the supervisory committee, and for their mentorship and support through my echocardiography training, and Dr. Surita Sidhu for her willingness participate as the 'arm's length' examiner. Your contribution to my education will not be forgotten. I also extend my gratitude to the Canadian Foundation of Innovation and Canadian Institutes of Health Research, which provided funding necessary to complete this work.

I would like to offer a very special thanks to my supervisor, Dr. Harald Becher, who has been an absolute pleasure to work with and learn from throughout my research fellowship and graduate studies. I truly could not have asked for a better mentor.

Table of Contents

List of Tables

List of Figures

Chapter 1, Figure 7: 3D rendering of the transducer/marker apparatus created through laser scanning allows determination of the geometrical relationship between the optical markers and transducer footprint (and by extension, the recorded 3DE pyramidal volume). Multiple perspectives of the transducer are shown.

Chapter 1, Figure 8: Demonstration of the relationship between the sonographer, patient, ultrasound scanner and infrared optical cameras in a typical optical tracking setup. A = OptiTrack V120™ pre-calibrated infrared optical camera system mounted on a tripod. Red arrows point to each of the 3 individual cameras. B = Ultrasound transducer shown (markers are not seen from this angle).

Chapter 1, Figure 9: M3DFE using optical transducer tracking. The optical tracking system documents the position and orientation of the transducers in three-dimensional space (an OptiTrack V120™ system is shown). The resulting ultrasound images are transformed onto a common coordinate system and subsequently fused. RA = Right Atrium, RV = Right Ventricle, LV = Left Ventricle, Ao = Aorta, PT = Pulmonary Trunk, Di = Diaphragm, Tr = Transducer with associated spherical optical markers.

Chapter 1, Figure 10: Cardiac excursion resulting from respiration. Note the dynamic relationship between the heart and transducer throughout the respiratory cycle. RA = Right Atrium, RV = Right Ventricle, LV = Left Ventricle, Ao = Aorta, PT = Pulmonary Trunk, Tr = Transducer. Modified from Punithakumar et al.(20).

Chapter 1, Figure 11: Top row: Multi-planar reconstruction of a single apical 3DE volume. Bottom row: Multi-planar reconstruction of a M3DFE volume generated from fusion of the above single apical 3DE volume plus one additional non-standard apical 3DE volume and a parasternal 3DE volume (total of three contributing 3DE volumes). Note the increased FOV characterized by enhanced visibility of the lateral LV wall and RV. Also note the improved image quality with enhanced endocardial border definition and reduced noise in the LV cavity.

Chapter 2, Figure 1: Steps required to produce a M3DFE dataset.

Chapter 2, Figure 2: The optical tracking device containing 3 infrared cameras (+tripod, left; zoomed view, right) used to track transducer and chest marker position in our study (OptiTrack V120:Trio, 6 degrees of freedom, resolution 640x480 x 3, refresh rate 120Hz). The height of the tripod ranged from approximately 120-150cm and was individualized to optimize the line of sight between the cameras and both the transducer and markers. Asterisks correspond to each of the three infrared cameras.

Chapter 2, Figure 3: Siemens 4Z1c matrix array transducer with mount/marker apparatus. Note the four silver spherical infrared markers attached to the mount (black). The 3D position and orientation of the markers (and by extension, the transducer) were tracked by the cameras through their preferential reflection of infrared light. The black mount was created using a 3D printer and consists of a plant-based, biodegradable and recyclable compound which is a blend of polylactic acid and polyhydroxyalkanoate (material by ColorFabb®).

Chapter 2, Figure 4: Chest markers affixed to the ECG stickers. These markers preferentially reflect infrared light in the same way the transducer markers do, allowing real-time monitoring of patient breathing and movement during echocardiographic recordings.

Chapter 2, Figure 5: M3DFE components and setup. A schematic diagram demonstrating the relationship between each of the necessary components (top center). The relative positions of the infrared cameras, ultrasound scanner, sonographer and study subject are shown (left). The computer used for 3D tracking and data collection is also shown (right).

Chapter 2, Figure 6: Fundamental frequency imaging was used for apical windows as near-field clutter artifacts seen with harmonic imaging (left) were much less prominent when imaging with fundamental frequencies (right).

Chapter 2, Figure 7: Screenshot of the M3DFE software viewer custom built for this project. A M3DFE volume comprised of one apical and one parasternal volume fused using the wavelet method is shown. Descriptions are seen in white text. MPR = Multi-planar reconstruction, ROI = Region of interest, 2D = 2-dimensional, FOV = field of view.

Chapter 2, Figure 8: 3D rendering of two M3DFE datasets illustrating favorable vs. unfavorable chest marker alignment. Left: An ideal M3DFE recording shows chest markers essentially superimposed on one another as demonstrated by the small white circles encompassing each set of markers. The mean chest marker displacement was 0.2mm in this case. This finding confirms the subject remained still and maintained an effective breath-hold maneuver and is predictive of successful spatial alignment. Right: A suboptimal M3DFE recording shows markers which are widely separated as demonstrated by the larger ellipses encompassing each set of markers. The mean chest marker distance was 4.5mm in this case, which is much greater than the 1.5mm threshold resulting in exclusion in this study, and is predictive of poor spatial alignment.

Chapter 2, Figure 9: Study design. This protocol was performed x 2 (end-systole + end-diastole). MPR = Multi-planar Reconstruction of 3DE volume. 2C = 2-chamber. 4C = 4-chamber.

Chapter 2, Figure 10: A M3DFE volume demonstrating poor alignment (left). Note the double-contoured interventricular septum. In this case, the mean chest marker displacement was 3.2mm – far greater than the threshold for exclusion of 1.5mm. The corresponding transducer/marker display is shown (right).

Chapter 2, Figure 11: Derivation of contrast, CNR and SNR values as shown here using an example multi-planar reconstructed 4-chamber view. Region of interest boxes were placed in the myocardium (red) and adjacent LV cavity (blue). Mean and standard deviations of pixel intensity within the regions of interest were used to automatically generate contrast, CNR and SNR values for each of the 6 standard myocardial segments in both the 4- and 2-chamber views.

Chapter 2, Figure 12: An example comparison of a non-fused single standard apical 3DE volume (top row), fused M3DFE consisting of the same standard apical 3DE volume as in the top row plus two additional non-standard apical 3DE volumes fused by the voxel averaging method (middle row) and fused using the wavelet method (bottom row). Note the enhanced myocardial signal / endocardial border definition, reduction in LV cavity noise, greatly improved visualization of the anterior wall (best seen in the 2-chamber view), and the increased FOV to display more of the right ventricle (best seen in the short-axis view). MPR = multi-planar reconstruction.

Chapter 2, Figure 13: An example comparison of a non-fused single standard apical 3DE volume (top row), fused M3DFE consisting of the same standard apical 3DE volume as in the top row plus both a non-standard apical volume 3DE and a parasternal 3DE volume fused by the voxel averaging method (middle row) and fused using the wavelet method (bottom row). Note the enhanced visibility of the RV and LV apex as well as the reduced noise seen with both fusion methods. Also note the diluted myocardial signal in the region of overlap that is characteristic of the fusion by averaging method (especially prominent in the interventricular septum). This is recovered when applying the fusion by wavelet decomposition method.

Chapter 3, Figure 1: Use of the ECG signal (black lines) and respiratory amplitude (blue lines) to perform respiratory gating on a multi-beat 3DE recording. Cardiac cycles are marked and the onset of the QRS complex (red dotted lines). Respiratory gating 'windows' are assigned

to times within the respiratory cycle where cardiac/diaphragmatic excursion is minimal, such as around end-inspiration or end-expiration. In this case, gating windows are shown at end-expiration (green parentheses). Those cardiac cycles falling within the respiratory gating window are eligible for fusion – two such cardiac cycles recorded from each of the apical and parasternal windows would represent ideal intervals for 3DE recording and subsequent fusion (green arrows).

List of Abbreviations

Chapter 1:

2D = 2-Dimensional

2DE = 2-Dimensional Echocardiography

3D = 3-Dimensional

3DE = 3-Dimensional Echocardiography

Ao = Aorta

CNR = Contrast-to-noise Ratio

CVD = Cardiovascular Disease

Di = Diaphragm

DSE = Dobutamine Stress Echocardiography

ECG = Electrocardiogram or Electrocardiographic

EM = Electromagnetic

ESC = Elevational Spatial Compounding

FOV = Field-of-view

LV = Left Ventricle/Ventricular

M3DFE = Multi-view 3D Fusion Echocardiography

PT = Pulmonary Trunk

RA = Right Atrium

RV = Right Ventricle

SNR = Signal-to-noise Ratio

Tr = Transducer

Chapter 2:

2C = 2-Chamber

2D = 2-Dimensional

2DE = 2-Dimensional Echocardiography

3D = 3-Dimensional

3DE = 3-Dimensional Echocardiography

4C = 4-Chamber

ANOVA = Analysis of Variance

AP = Apical-parasternal (imaging protocol)

AVG = Fusion by Voxel Averaging (M3DFE imaging group)

CNR = Contrast-to-noise Ratio

EBD = Endocardial Border Definition

FOV = Field-of-view

HSD = Honest Significant Difference

LV = Left Ventricle/Ventricular

M3DFE = Multi-view 3D Fusion Echocardiography

MPR = Multi-planar Reconstruction

NSA = Non-standard Apical (imaging protocol)

ROI = Region of Interest

SNR = Signal-to-noise Ratio

SSA = Single Standard Apical (non-fused imaging group)

UNM = Unmoving Transducer (imaging protocol)

WAV = Fusion by Wavelet Decomposition (M3DFE imaging group)

Chapter 3:

3DE = 3-Dimensional Echocardiography

CCT = Cardiac Computed Tomography

CMRI = Cardiac Magnetic Resonance Imaging

EM = Electromagnetic

FOV = Field-of-view

LA = Left Atrium

LV = Left Ventricle

M3DFE = Multiview Fusion 3D Echocardiography

RV = Right Ventricle

TEE = Transesophageal Echocardiography

Chapter I

Multi-view 3D Fusion Echocardiography:
Background and Literature Review

1. Current Use and Limitations of Transthoracic 2D and 3D Echocardiography

2-dimensional echocardiography (2DE) is by far the most commonly used cardiac imaging modality, owing to its widespread availability, portability, versatility, relatively low cost, exceptional safety profile and excellent temporal and spatial resolution (1-4). 2DE is almost always the first-line test for assessing cardiac structure and function. However, 3D echocardiography (3DE) affords the viewer a more realistic and lucid appreciation of complex cardiac anatomy and is considered the echocardiographic method of choice for assessing left ventricular (LV) systolic function according to the American Society of Echocardiography (5, 6). Two of the most important advantages of chamber quantification using 3DE versus 2DE are i) the elimination of geometric assumptions inherent to 2DE, and ii) the ability to avoid LV apical foreshortening (5). LV quantification with 3DE is also more reproducible and accurate than with 2DE (5).

3DE does, however, have significant limitations. These limitations include i) increased noise, ii) increased ultrasound attenuation, and iii) reduced contrast versus 2DE. These limitations are, at least partially, explained by the inherently reduced spatial resolution generated by 3DE versus 2DE transducers (5, 7). Additionally, temporal resolution is inherently reduced with 3DE compared to 2DE, which can result in an inability to visualize cardiac structures during true end-diastole or end-systole, thereby introducing possible errors in chamber quantification (5). Field-of-view (FOV) is reduced as part of a trade-off to maintain diagnostic line-density/spatial resolution and volume-rate/temporal resolution, and contributes to an enhanced dependence on the favorable acoustic windows often required to generate useful images (8). Special expertise is required to acquire, process and interpret 3DE recordings, and this can have implications for workflow and laboratory efficiency.

Perhaps the most important limitation to 3DE is not unique to 3DE but applies to echocardiography in general. Weakly reflected signals from important cardiac structures are often the result of non-perpendicular angles of insonation. This results in suboptimal endocardial border definition and is particularly problematic when performing LV quantification, which must be performed from the apical window since it is the only window from which the entire LV is visualized (7, 9).

2. Addressing the Limitations of Transthoracic 3D Echocardiography

2.1 Non-fusion Techniques

A number of technological advancements have helped mitigate some of the limitations of 3DE described above. 3DE transducers with smaller footprints have been developed, leading to enhanced acoustic access and ease of use by sonographers (8). Automated adaptive analytics algorithms have been created which automatically perform cardiac chamber quantification to reduce manual post-processing time and improve workflow efficiency (10, 11). While it does not address the issue of reduced spatial and temporal resolution or tangential angles of insonation, contrast 3DE can improve visibility by improving left ventricular endocardial border definition and quantification in those with poor acoustic windows (8). The above methods are all examples of '*non-fusion'* based techniques that can be applied to improve the diagnostic potential of 3DE.

2.2 Fusion Techniques

In addition to the above advancements, an imaging technique termed echocardiographic '*fusion*' has been investigated to help address the limitations of 2DE and 3DE. Image fusion is not a novel concept. It has been used to study a variety of organs and applied to multiple imaging modalities (12-16). In cardiology, image fusion has been used to integrate complementary information from both intramodality and intermodality perspectives (12, 17, 18).

In echocardiographic fusion, separate datasets are superimposed, or 'fused', in an effort to improve image quality and measurement reproducibility. Enhanced image quality results

from i) enhanced contrast, ii) suppression of noise, iii) improved contrast-to-noise and signal-to-noise ratios and iv) reduced imaging artifacts such as acoustic shadowing and reverberation (4, 19-22). It should be noted that 'fusion' has been described using various terms depending on the technique used and the publication being reviewed. 'Compounding', and 'mosaicking' are alternative terms that, in the proper context, are synonymous with 'fusion' as described above (4, 6, 23-26).

2.3 'Single-view' Fusion Echocardiography

Two examples of early single-view fusion techniques studied with 2DE are elevational spatial compounding (ESC) and temporal compounding (4, 24, 27). A more recent approach to 3DE fusion that is now widely used in 3DE is the multi-beat 3D 'full-volume' acquisition. Both of these techniques fuse datasets obtained from a single transducer location and can therefore be considered *'single-view'* fusion techniques.

2.3.1 Elevational Spatial Compounding

In ESC, 2DE datasets are recorded from a stationary transducer that is angulated through a small arc above and below a set neutral position (in the *elevational* plane) over multiple cardiac cycles (23, 24, 27). In a post-processing procedure, datasets from the same part of the cardiac cycle (e.g. end-diastole) but generated from subtle incremental transducer angulations over multiple beats are fused to provide a single 2DE dataset. The resulting product demonstrates i) reduced noise, ii) enhancement of weak signals to improve contrast, iii) improved signal-noise ratios and iv) reduced artifacts (23, 24, 27, 28).

An important limitation of ESC is that the nature of the technique predisposes to tissue boundary blurring with progressively increased sizes of the elevational plane arcs used in the compounding process (24). This effect is more pronounced in the far field because of the greater absolute ultrasound beam excursion for a given change in probe angulation (24). The resultant tissue boundary blurring can confound chamber quantification, with cardiac chambers appearing smaller than their true size (4, 24). It may also be more difficult to differentiate the compact and trabeculated myocardium, and may actually *increase* artifacts

if the elevational angle is large enough that structures such as adjacent lung or bone are captured in the imaging arc.

Furthermore, ESC does not address the limitation of suboptimal angles of ultrasound incidence relative to surfaces of interest because the transducer records from a single acoustic window. Nonetheless, ESC is a relatively simple technique, and some software programs already employ a variation of this technique in the post-processing of 3DE datasets during multi-planar reconstruction through manipulating a 2DE plane's 'slice thickness'. Using matrix-array transducers, it is also possible to perform ESC in real-time to generate 2DE displays with enhanced image quality. However, routine clinical use of ESC in this context requires further validation studies on human subjects (24).

2.3.2 Temporal Compounding

In temporal compounding, datasets taken from an unmoving transducer are fused from either i) multiple temporally adjacent frames within a single cardiac cycle, or ii) similarly-timed frames from different cardiac cycles (4, 27-29).

In the first case, where datasets from a single cardiac cycle are fused, the result is an image with reduced noise, improved signal-noise ratio, and a subjectively 'smoother' appearance (28) . These benefits generally come at the expense of a reduction in temporal resolution that can range from subtle to dramatic, depending on the compounding technique and decided number of successive frames to be fused. Also, since the heart is a moving structure, a variable degree of tissue boundary blurring occurs (28). As such, this method is most helpful in the assessment of slow-moving structures, and much less helpful for fast-moving structures such as cardiac valves. Real-time temporal compounding performed in this manner is an available feature termed 'persistence' on most currently available echocardiographic ultrasound scanners.

In the second case, similarly timed datasets from different cardiac cycles are fused (4). This approach takes advantage of the similarity in cardiac anatomy and motion over successive cycles. Using this method, similar benefits are achieved without sacrificing temporal resolution. The drawback is that, given the acquisition occurs over multiple beats, even minor movements/slippage of the transducer can significantly worsen the effects of tissue boundary blurring to negatively impact image quality and the diagnostic value of the compounded

dataset (28). Breath-hold maneuvers to minimize the effects of respiration on cardiac position, and a regular heart rhythm are also required (28).

2.3.3 Multi-beat 3D Full-volume Echocardiography

Single-view fusion has also been applied to 3DE. In a technique called 'multi-beat 3D full-volume' echocardiography, a multi-beat recording is acquired from a single transducer position, with each individual beat giving rise to a 'sub-volume'. Sub-volumes are then fused or 'stitched' together into a 'full-volume' with pyramidal dimensions of up to 90° x 90°. The result is an improved field-of-view (FOV) while maintaining high temporal and spatial resolution (8)(Figure 1). Typically, 2, 4 or 6 heart beats are used to create a full-volume dataset (8). The greater the number of beats or sub-volumes acquired, the better the temporal and spatial resolution of the final full-volume dataset. The unfortunate trade-off is potential 'stitching' artifacts, which are more apparent when progressively more heart-beats are used in the multi-beat acquisition.

'Stitching' artifacts are due to spatial misalignment of sub-volumes. They result from beat-to-beat variations in heart rate or cardiac position (30). Changes in cardiac position relative to the transducer result from either patient or transducer movement, or patient respiration. The ideal acquisition therefore occurs during a breath-hold maneuver in a stationary patient with a regular heart rhythm – conditions that are sometimes difficult or impossible to achieve unless the patient is sedated or anesthetized. These limitations are especially problematic given the number of patients in a typical cardiology practice who may have difficulty cooperating with the above measures, or who may have atrial fibrillation, frequent ectopy or other arrhythmias.

2.4 Weakness of Single-view Fusion Echocardiography

Given that all of the above methods utilize fusion based on datasets acquired from a stable transducer position, or 'single-view', they do not solve the problem of limited cardiac visibility or tangential angles of insonation relative to the LV endocardial border. As such, even though signal-to-noise ratios can be improved, and artifacts can be reduced, endocardial border definition and FOV remain suboptimal using these approaches.

3. Multi-view 3D Fusion Echocardiography

While in single-view fusion echocardiography the transducer remains in a *single position* throughout data acquisition, transducers from *multiple positions* are used to create fusion datasets in multi-view 3D fusion echocardiography (M3DFE) (12, 21, 31). The goal is to fuse two or more datasets that, by virtue of being generated from different acoustic windows, contribute redundant but complementary information to the resulting image. Figure 2 demonstrates one method of performing M3DFE where multiple different transducer positions situated around the cardiac apex are used to generate a fusion dataset (21).

Understanding the following concept can help one understand how these redundant yet complementary datasets are fused to improve overall image quality for a structure of interest, such as the LV. The LV myocardium and endocardial borders at the mid and base are often best appreciated from the parasternal window owing to the relatively perpendicular angle of ultrasound incidence between the transducer and LV endocardial border when viewed from this perspective. This is in stark contrast to the highly tangential, sometimes almost parallel, angles of incidence between the ultrasound beam and endocardial border observed when imaging from the apical window (Figure 3) (9, 32). However, despite this strength of the parasternal window, the apex is almost never completely visualized. As such, clinicians are forced to rely upon the apical window for LV quantification, as it is the only window that allows complete LV visualization.

Using M3DFE, parasternal and apical 3D volumes can be fused, resulting in a fusion dataset that combines the strength of the parasternal window (optimal endocardial border definition at the mid and base of the LV) with the strength of the apical window (visualization of the cardiac apex and entire LV) (9). The result is a dataset with improved overall image quality and diagnostic power compared to either dataset alone (9). A graphic summary of this concept is provided in Figure 4. A M3DFE example demonstrating fusion of parasternal and apical volumes to produce a dataset of greater image quality and FOV than either alone is shown in Figure 5.

The potential benefits of M3DFE are many. Since the heart is viewed from more than one perspective, FOV is enhanced without sacrificing spatial or temporal resolution. A clinical example of where this would be helpful is during the examination of patients with large hearts.

In some cases, a person's LV or right ventricle (RV) is so large that it is difficult to fit into the FOV. This is particularly problematic when trying to perform LV quantification on an individual with a dilated cardiomyopathy using 3DE, where flexibility to enhance FOV while maintaining spatial and temporal resolution is already limited. Accuracy of LV quantification might be enhanced if parasternal windows are fused with apical ones, as these M3DFE datasets should demonstrate improved endocardial border definition owing to perpendicular angles of insonation from the parasternal window. An improvement in LV quantification may reduce the need for routine contrast administration – a procedure which ubiquitously impacts the workflow and budgets of echocardiography laboratories. These are just a few reasons why M3DFE has gained the interest of many investigators.

The benefits of M3DFE are not achieved easily. Multiple steps are required to successfully create a diagnostic-quality M3DFE dataset. These steps can be broadly divided into i) spatial alignment, ii) temporal alignment and iii) image fusion and optimization (Figure 6) (21, 22, 33). Just as in single-view fusion echocardiography, successful creation of a M3DFE dataset generally requires that the patient has a regular heart rhythm, can remain still, and can perform breath-hold maneuvers during data acquisition. The following section will expand upon each of these individual steps.

4. Spatial Alignment

The first step in performing dataset fusion is to decide how echocardiographic datasets will be spatially aligned. There are two broad categories of spatial alignment techniques: spatial alignment by *image registration* and spatial alignment by *transducer tracking*.

4.1 Spatial Alignment by Image Registration

In spatial alignment by *image registration*, computer algorithms are used to determine the optimal spatial alignment of two or more datasets (1, 12, 21). Registration algorithms used for 3DE include i) feature-based registration, ii) optical flow-based methods, iii) feature-based methods and iv) voxel-wise similarity measures (14, 34). A comprehensive technical description of the various image registration methodologies is beyond the scope of this review but can be found elsewhere (1, 6, 14, 34). Image registration has been extensively investigated

and has been the most widely studied method of spatially aligning datasets. It has been used in the fusion of echocardiographic datasets, and also in the fusion of datasets across different imaging modalities (12, 32, 35-39).

While spatial alignment by image registration can be highly effective, several important limitations exist: i) registration performs best when aligning datasets with a significant degree of similarity or large area of overlap (such as those obtained from two or more similarly located apical windows from where structures' orientation and appearance are similar, as seen in Figure 2) (21, 40). However, registration is more challenging when attempting to align significantly different datasets with limited overlap, such as those obtained from distantly located transducer positions (i.e. from apical and parasternal windows where differential angles of insonation result in changes in an objects' appearance). This is problematic because the greatest potential benefits of M3DFE are realized when datasets from remote acoustic windows are fused (19, 20, 41); ii) the accuracy of alignment by image registration is limited by the resolution of the datasets themselves, which is usually about 1mm for 3DE; iii) individual datasets are prone to artifacts and noise that can confound proper spatial alignment (42); iv) the heart is a dynamic or 'non-rigid' structure, and if fusion of cine loops is desired (rather than still volumes), computer analysis is sophisticated and computationally expensive (14, 20, 41, 42). However, limitations i) and iii) are being addressed through the active study of increasingly sophisticated and successful registration algorithms for spatial and temporal alignment, such as approaches utilizing atlas-based mosaicking and similarities in image features (eg. using scale invariant feature transform features)(6, 34, 43); limitation iv) is mitigated by contemporary computer systems using increasingly powerful graphics processing units and efficient algorithms. It is therefore fair to expect that the versatility and effectiveness of registration techniques will only continue to improve with time.

4.2 Spatial Alignment by Transducer Tracking

Because of the significant limitations of image registration some research laboratories have shifted focus to a different approach based on tracking of the transducer in 3D space. In spatial alignment by transducer tracking, 3D spatial coordinates of the transducer are monitored and recorded, and datasets are aligned and fused based on this data. Importantly,

in contrast to alignment using image registration, alignment by transducer tracking does not rely upon visual similarity between datasets.

Spatial alignment of datasets by tracking of the transducer alone only works if the position of the heart in 3D space is stable. However, the heart's position in 3D space moves as a result of the effects of respiratory excursion of both the diaphragm and the chest wall (32). Moreover, the heart's location with respect to the chest cavity changes with breathing and with body position. A successful M3DFE study, therefore, accounts for these factors and this is discussed in greater detail later in this section.

To date, two major tracking methods have been investigated to track transducer position and orientation: i) optical tracking and ii) electromagnetic (EM) tracking. Each will be described in the following two sections.

4.2.1 Optical Tracking

In optical tracking, special cameras track the position and orientation of an object of interest by emitting infrared light that is reflected back to the cameras by specially designed markers affixed to the object of interest. Optical tracking has many diverse applications in medicine, ranging from guidance of endoscopic procedures to intraoperative electron radiation therapy (44, 45).

When used for echocardiographic fusion, multiple cameras track the position of optical markers affixed to an ultrasound transducer. The markers must be multiple (at least three) and must be asymmetrically oriented. Both the *position* and *orientation* of the transducer are recorded and tracked once the cameras detect the markers in their expected configuration. The position and orientation of the corresponding 3D pyramidal volume is then determined using the known geometric relationship between the optical markers and transducer footprint (Figure 7). The pyramidal sound-field emitted from the transducer is assumed to arise symmetrically from a central point on the footprint. Of note, while previous versions of optical tracking systems required a cumbersome calibration procedure before each use, recent systems such as the Optitrack V120:Trio™, are designed in such a way that the system is pre-calibrated (a typical setup is shown in Figure 8).

During 'transformation', the position and orientation of each contributing pyramidal volume are assigned Cartesian coordinates according to X, Y and Z axes. Successful

transformation results in accurate spatial alignment of cardiac structures from contributing volumes and is the final step before dataset fusion (Figure 9) and subsequent image processing and optimization.

A major strength of optical tracking is that it is highly accurate – even sub-millimeter transducer displacements can be reliably detected, with accuracies as good as approximately 0.2-0.5mm (20, 42, 46, 47). Despite typical axial and lateral resolutions of 1mm and 2mm respectively for typical real-time 3DE, this sub-millimeter accuracy is important because even minute errors in the detected location of the transducer can have drastic effects in the recorded location of objects, especially in the far-field of the sound-field given the wide divergence of ultrasound beams (48).

The major downfall of optical tracking is the line-of-site limitation. If an object intercepts the line-of-sight between the camera and the marker, the 3D position of the transducer may be lost (20). This limitation is of great importance as most echocardiographic scans require a diverse range of transducer-sonographer-patient relationships to obtain high quality datasets. Also, in the spirit of maintaining patient modesty during examinations, towels or sheets are often placed between the sonographer and patient with the very intention of obstructing line-of-sight, especially when imaging female patients. Consequently, the transducer may be moved into positions that result in a loss of line-of-sight between the camera and transducer. Use of multiple cameras placed at different heights and positions about the patient have been used in an effort to minimize this limitation (42). However, situations where line-of-sight would remain obstructed, regardless of the number of cameras used, are inevitable.

Another limitation of optical tracking is the bulky mount containing the 3D markers that must be affixed to the transducer. The bulky transducer-marker apparatus can make obtaining high quality images challenging if the markers obstruct the sonographer's ability to maneuver the transducer into a particular required position. Not all markers are bulky, however. Some systems exist where multiple paper-thin markers are stickered onto the transducer's surface, effectively eliminating the problem of a bulky transducer-marker apparatus but with the potential trade-off of a greater difficulty maintaining line-of-sight (49).

4.2.2 Electromagnetic Tracking

In EM tracking, magnetic sensors are localized within a magnetic field of known geometry (50). The magnetic field can be generated by either permanent magnets or via electromagnetism (50). A magnetic sensor is affixed to an object of interest to be tracked, and also connected to a tracking computer by means of a flexible wire.

In the setting of echocardiography, magnetic sensors are affixed to the ultrasound transducer and connected to an external computer via a thin flexible wire. A field generator is positioned in the vicinity of the transducer, usually just above the patient's chest. The 3D position and orientation of the transducer is then tracked by the tracking computer (41, 51). In a similar manner to that used in optical tracking, the known geometric relationship between the sensor(s) and transducer footprint allows for determination of the position and orientation of the echocardiographic 3D pyramidal volume. Once this information is gathered, transformation and alignment can be performed. The feasibility of echocardiographic EM tracking performed in this fashion has been demonstrated in prior studies using both 2DE and 3DE models (41, 51, 52).

EM tracking has the advantage of avoiding the line-of-site limitation and bulky markers associated with optical tracking. Unfortunately, there are significant limitations to EM tracking. First, EM tracking can be significantly affected by even weak local magnetic fields (50). This is problematic because many echocardiographic laboratories are situated near medical devices such as magnetic resonance imagers or other magnetically active systems. In this sense, EM tracking is less robust than optical tracking, which is impervious to such effects. Second, wires must connect the transducer and sensing computer. Third and perhaps most importantly, the accuracy of EM tracking is inferior to optical tracking. The accuracy of EM and optical tracking is approximately 1.0 – 1.4mm and 0.2 – 0.5mm, respectively, which is important for the reasons described above in section 4.2.1 (20, 46, 50).

4.2.3 Accounting for Patient Movement

A successful M3DFE study requires that patient movement is accounted for, as even small changes in body position can greatly affect the spatial relationship between the heart and the transducer. To date, this has been accomplished by acquiring 3D datasets with subjects remaining still. Prior to recording each 3DE dataset, it is possible to confirm a stable body position through the quantitative and/or qualitative monitoring of optical markers or

magnetic sensors affixed to the chest wall. However, this method of confirming stable position has not been extensively studied and warrants further investigation.

5. Temporal Alignment

Both the heart's position and morphology change with cyclical variations in the respiratory and cardiac cycles. As such, this must be accounted for in order to effectively fuse echocardiographic datasets. Each of these two factors are described in the following sections.

5.1 Accounting for the Cardiac Cycle

Each contributing dataset in a M3DFE study must be synchronized according to the cardiac cycle. Synchronization of datasets according to the cardiac cycle is commonly performed by manual selection, electrocardiographic (ECG) gating, or by using ECG-independent temporal registration algorithms (20, 34, 53). Temporal alignment is more challenging when there are differences in the durations of cardiac cycles between contributing 3DE recordings, as even subtle variations in heart rate can result in differing total volumes per recording. If the difference is minor, one or two volumes for example, this can be accounted for by truncating the longer recording(s) by one or two volumes so the total number of volumes remains constant. Alternatively, temporal interpolation techniques can be applied to generate interpolated frames which can be used to create an exact temporal match between recordings. This approach requires further validation studies as there is potential to introduce additional artifacts due to inconsistencies in pixel intensities between successive volumes which result from noise. However, it does offer a potential strategy which might address the variations in heart-rate encountered in patients with arrhythmias.

5.2 Accounting for Patient Respiration

The location of the heart within the body changes significantly throughout the respiratory cycle, owing to movement of both the diaphragm and chest wall (Figure 10) (14, 32, 54, 55). During regular tidal respiration, the heart is displaced as much as 10-20 mm, with most movement occurring in the craniocaudal direction (55, 56). As such, it is imperative that these

changes are considered when performing M3DFE. Imaging modalities which directly visualize the diaphragm, such as cardiac computed tomography (CCT) and cardiac magnetic resonance imaging (CMRI), can compensate for respiratory motion through directly monitoring and then correcting for diaphragmatic movement (57, 58). However, unlike in CCT and CMRI, echocardiography is not afforded the luxury of reliable visualization of diaphragmatic movement. The most simplistic way to account for respiratory motion in M3DFE involves minimizing diaphragmatic movement by recording datasets during breath-hold maneuvers at either end-inspiration or end-expiration (20). For now, M3DFE has generally been studied in the setting of such breath-hold maneuvers. However, future approaches employing more sophisticated 'respiratory-gating' techniques could allow M3DFE dataset acquisition during free-breathing, a feature that would be important to promote M3DFE's adoption into mainstream clinical practice.

6. Fusion of Overlapping 3DE Volumes

The final step in M3DFE is to process overlapping portions of individual 3DE recordings to generate the M3DFE dataset. Specifically, one must determine the final intensity of each voxel (3D equivalent of pixel) in the region of overlap. Numerous approaches have been studied, each utilizing its own unique computer algorithm. A comprehensive explanation of the various fusion methods is beyond the scope of this review but can be found elsewhere (19, 20, 59, 60). Briefly, intuitive methods which use the mean or maximum voxel intensity from contributing datasets are easy to implement. However, it has been observed that fusion by voxel averaging often impairs contrast and fusion by maximum voxel intensity reduces signal-to-noise ratio (20, 60). A technique called wavelet decomposition has demonstrated promising results in some studies. This technique divides, or 'decomposes', an image volume into its high- and low-frequency components and subsequently suppresses the visualization of high frequency components (assumed to contain noise and artifacts). This leads to a relative enhancement of the low-frequency components which contain signals of interest such as the myocardium (19, 20). The result is increased contrast and contrast-to-noise ratio (20, 60). It is important to note that, despite the promising results of fusion by wavelet decomposition in some studies, there is still no clear consensus on which fusion algorithm consistently yields the best results.

7. Results of Human M3DFE Studies

To the best of our knowledge, there have been 18 publications demonstrating the feasibility of M3DFE in humans, the vast majority of which have been in a *pre-clinical* setting using healthy volunteers (Table 1). The overarching benefits of M3DFE noted in these studies are an extended FOV and enhanced image quality. An example demonstrating improved FOV and image quality with M3DFE is shown (Figure 11). Studies have been performed using commercially available 3DE scanners such as the Philips iE33 and Siemens Acuson SC2000. To our knowledge, all have relied on breath-hold maneuvers to account for respiratory motion.

Importantly, the accuracy of measurements made using M3DFE are not negatively impacted. In one study investigating the accuracy of data produced by M3DFE, LV volumes and ejection fractions derived from M3DFE showed similar agreement with CMRI values as those derived from real-time 3DE (21). This supports the notion that M3DFE performs at least as good as conventional real-time 3DE on measures of LV chamber quantification.

Most studies have used various image registration techniques to spatially align M3DFE datasets – only a small minority of recent studies have investigated spatial tracking in place of registration. Successful registration generally requires significant similarity/overlap of 3DE datasets (although some recent techniques are challenging this as described in section 4.1), and the greatest strength of M3DFE comes from the fusion of complementary 3DE datasets generated from distantly located acoustic windows. However, only 6 studies have investigated fusion of the distantly located apical and parasternal windows.

8. Current Challenges with 3D Fusion Echocardiography

A select few laboratories have studied M3DFE for many years. Nonetheless, M3DFE is still a relatively novel technology. While M3DFE offers many important benefits over standard 3DE, it is technically challenging. Multiple steps are required in order to produce diagnostic quality M3DFE datasets. Current fusion software programs require special expertise, and an optimal / clinically feasible alignment and fusion protocol has not been defined. Alignment, fusion and analysis must be performed offline in a similar manner to standard 3DE and can be time-consuming. This might have implications on work-flow in busy laboratories. However, M3DFE technology will almost certainly become more efficient as it is developed further.

As mentioned above, the vast majority of data on M3DFE is based on small pre-clinical studies recruiting healthy volunteers which lend to ideal sonographic conditions. There is a paucity of data on those with structural heart disease, and in patients that are technically challenging to scan. Studies of M3DFE in these settings, which include validation assessments comparing results of volumetric analysis by M3DFE to gold standard techniques like CMRI, are required before M3DFE is ready for mainstream clinical use.

Despite these challenges, promising techniques have emerged which have the potential to significantly advance M3DFE. In particular, spatial alignment using transducer tracking and sophisticated new registration techniques show great promise as these methods do not rely on significant data overlap and can therefore be used to exploit the greatest advantage of M3DFE – fusing datasets obtained from remotely located acoustic windows. Encouragingly, these techniques are expected to evolve to become progressively more robust and accurate in the ensuing years.

9. Conclusion

There is a growing body of evidence supporting the notion that M3DFE helps overcome current limitations of 3DE to improve image quality and FOV by fusing complementary 3DE datasets. Although M3DFE is still an emerging technology, recent advancements have improved its feasibility, accuracy and robustness. We therefore believe M3DFE is ready for further clinical trials in healthy volunteers as well as in individuals with cardiac disease.

10. Chapter 1 Tables and Figures

Author, Year of Publication	Study Subjects	Spatial Alignment Method	Pertinent Findings
P. Soler et al., 2005 (40)	8 subjects	Registration of slightly offset multiview transthoracic apical 3DE datasets	Extended FOV, improved contrast and SNR
V. Grau et al., 2007 (1)	9 subjects	Registration of multiview transthoracic apical and parasternal 3DE datasets	Demonstration of feasability of novel algorithm used to register apical and parasternal datasets
V. Grau et al., 2008 (9)	3 healthy subjects	Registration of multiview transthoracic apical and parasternal 3DE datasets	Improved endocardial contour tracking using multi-view versus single-view datasets
K. Rajpoot et al., 2009 (61)	12 healthy subjects	Registration of multiview transthoracic standard and non-standard apical 3DE datasets	Filling in of missing anatomical information, extending FOV and increasing structural information and image contrast
C. Szmigielski et al., 2010 (21)	32 healthy volunteers	Registration of multiview transthoracic standard and non-standard apical 3DE datasets	Improved endocardial border detection, overall image quality, SNR, CNR and FOV
M. Gooding et al., 2010 (60)	7 healthy pregnant volunteers	Registration of 3-8 fetal 4D spatiotemporal image correlation datasets per volunteer	Improved image quality by both qualitative and quantitative measures; improved reproducibility of semiautomated LV segmentation
K. Rajpoot et al., 2011 (19)	36 healthy subjects	Registration of multiview transthoracic standard and non-standard apical 3DE datasets	Improved contrast, CNR, SNR, anatomic features and FOV

K. Rajpoot et al.,2011 (7)	34 subjects	Registration of multiview transthoracic standard and non-standard apical 3DE datasets	Improved automated LV segmentation and tracking, improved FOV
C. Yao et al., 2011 (62)	10 volunteers, 2 patients	Registration of multiview transthoracic apical and parasternal 3DE datasets with the aid of optical transducer tracking	Qualitatively improved FOV, image quality, endocardial definition; reduced cavity noise; quantitatively improved SNR and contrast
Ren et al., 2013 (63)	8 cardiac surgical patients	Registration of multiview transesophageal 3DE datasets	Extended FOV of the LA to include important landmarks such as the pulmonary vein's, left atrial appendage, mitral and aortic valves and fossa ovalis in one fused 3DE dataset
G. Piella et al., 2013 (64)	8 volunteers and 1 patient	Registration of multiview transthoracic apical and parasternal 3DE datasets with the aid of optical transducer tracking	Improved consistency of strain curves and reduced number of segments demonstrating non-physiologic strain patterns
D. Augustine et al., 2015 (22)	24 subjects referred for DSE to investigate possible CVD	Registration of 3 multiview (transducer rotated through 4-, 2- and 3- chamber reference planes) transthoracic 4-beat 3DE *full-volume* apical datasets per patient (all performed at rest)	Fused 3D volumes showed significantly improved CNR and segmental image quality versus unfused volumes, at levels close to that achieved by 2D contrast echocardiography
Carminati et al., 2015 (65)	17 patients	Registration of multiview transesophageal 3DE datasets of the descending thoracic aorta	Demonstrated the feasibility and accuracy of this approach to create 3D reconstructions of the descending thoracic aorta and quantify atheroma burden; extended FOV
K. Punithakumar et al., 2016 (20)	6 healthy subjects	Optical spatial alignment of multiview transthoracic apical and parasternal 3DE datasets	Improved FOV, contrast, CNR, SNR and feature count

A. Danudibroto et al., 2016 (6)	10 healthy subjects	Registration to fuse 4-8 multiview transthoracic 3DE datasets located about the LV and RV apex	Demonstrated feasibility and accuracy of novel temporal and spatial registration techniques
J Bersvendsen et al., 2016 (34)	16 patients with aortic insufficiency	Spatial and temporal registration of transthoracic apical 3DE datasets	Demonstrated feasibility of temporal alignment (by normalized cross correlation over time functions) *and* spatial alignment (by 3D scale invariant feature transform features) in a clinical population
D. Peressutti et al., 2017 (25)	4 healthy subjects	Registration of multiview transthoracic (modified parasternal + apical) 3DE datasets	Subspace error metric registration outperforms sum-of-squared differences and phase-based error metrics in terms of accuracy, robustness and execution time
H Mulder, et al., 2017 (43)	16 cardiac surgical patients	Registration of multiview transesophageal 3DE recordings using atlas-based mosaicking	Demonstrated feasibility and improved registration robustness and smaller registration errors compared with regular pairwise registration

Table 1: Key pre-clinical and clinical studies assessing 3D echocardiographic fusion. DSE = dobutamine stress echocardiography, CVD = cardiovascular disease, CNR = contrast-to-noise ratio, SNR = signal-to-noise ratio, FOV = field-of-view.

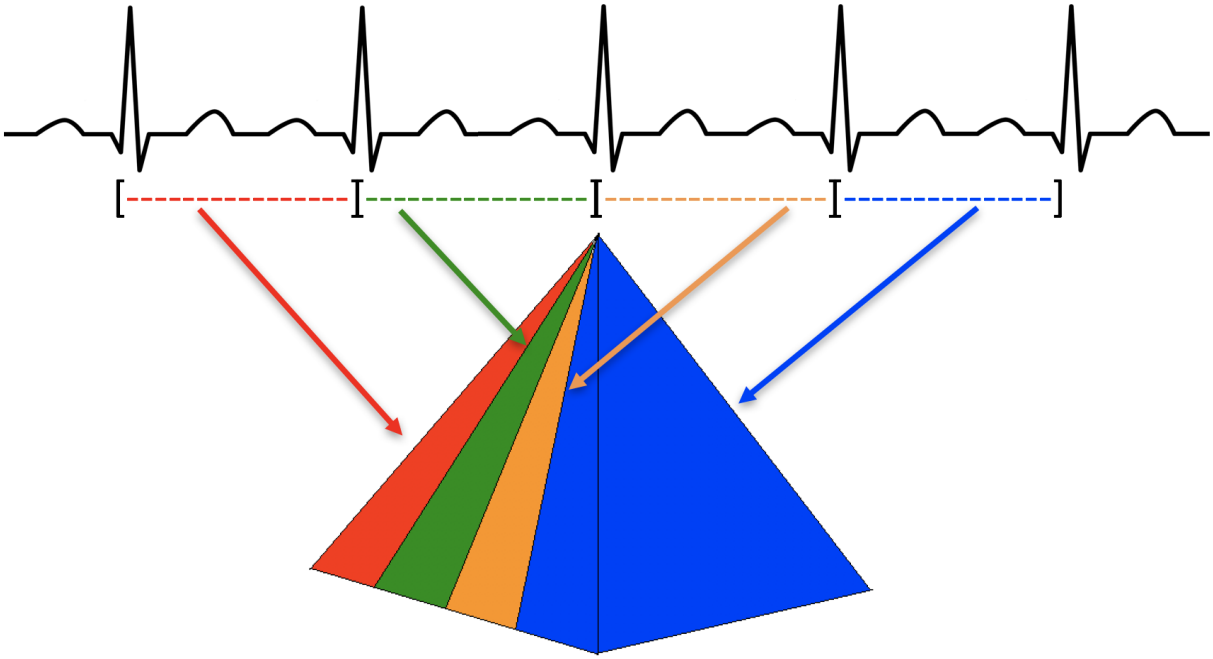

Chapter 1, Figure 1: Multi-beat 3DE full-volume acquisition. Each color represents one sub-volume, with each being created from a different cardiac cycle. Modified from Lang et al. (13).

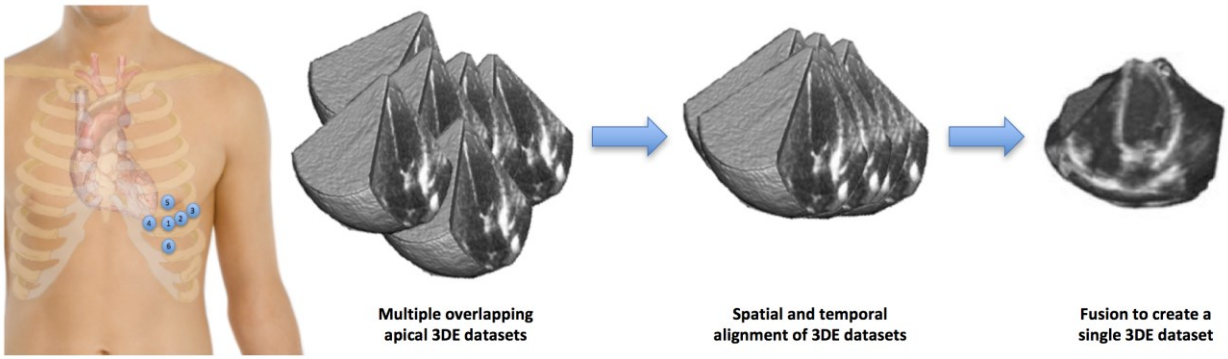

Chapter 1, Figure 2: Fusion of multiple 3DE datasets acquired from overlapping standard and non-standard apical windows. Once datasets are spatially and temporally aligned, they are fused into a single 3DE dataset.

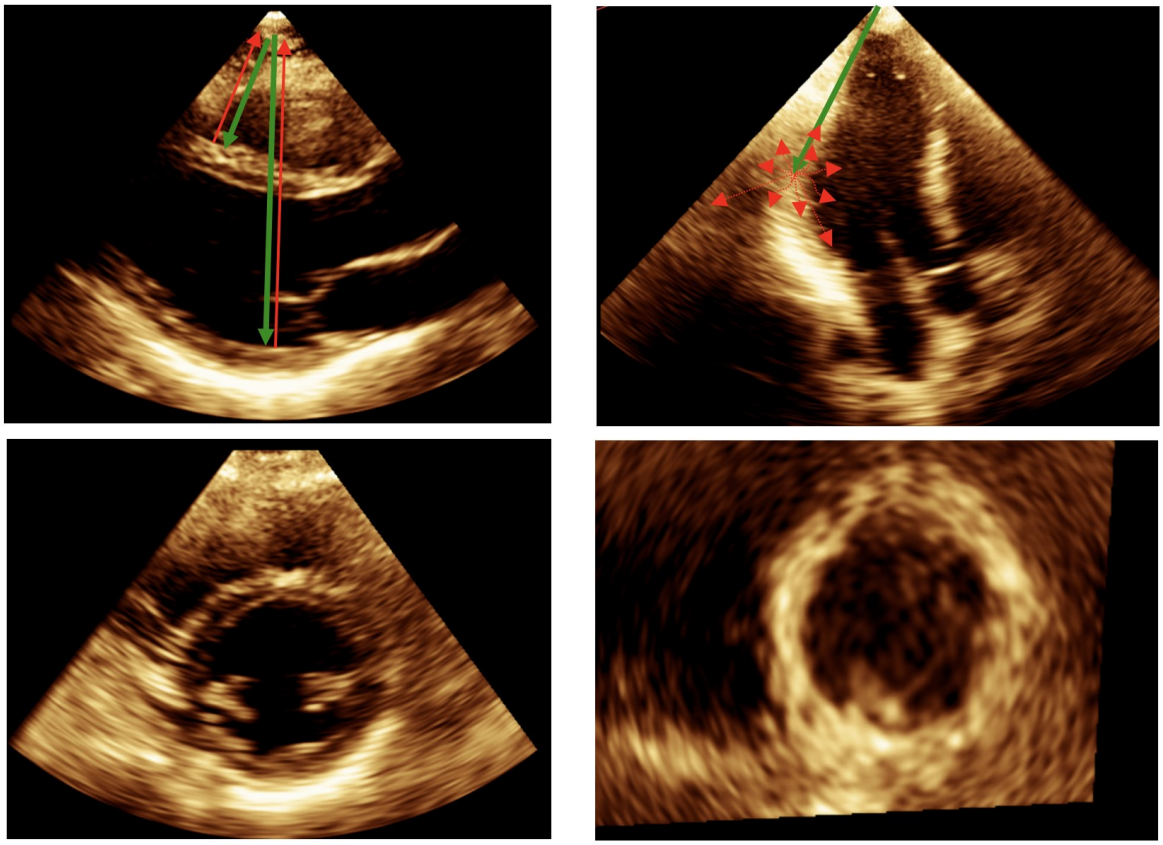

Chapter 1, Figure 3: Endocardial border definition as viewed with multi-planar 3DE reconstructions from parasternal vs. apical windows. Endocardial border definition at the mid and base of the left ventricle is superior from the parasternal window owing to a relatively perpendicular angle of ultrasound beam incidence relative to the endocardial border. Endocardial border definition is reduced at the mid and base of the left ventricle as viewed from the apical window, owing to relatively tangential angles of ultrasound incidence. Top images = long axis; bottom images = short axis. Thick green arrows represent the incident ultrasound beam. Thick red arrows represent strong ultrasound signals resulting from specular reflection. Dotted red arrows represent weak ultrasound signals resulting from diffuse reflection or backscatter.

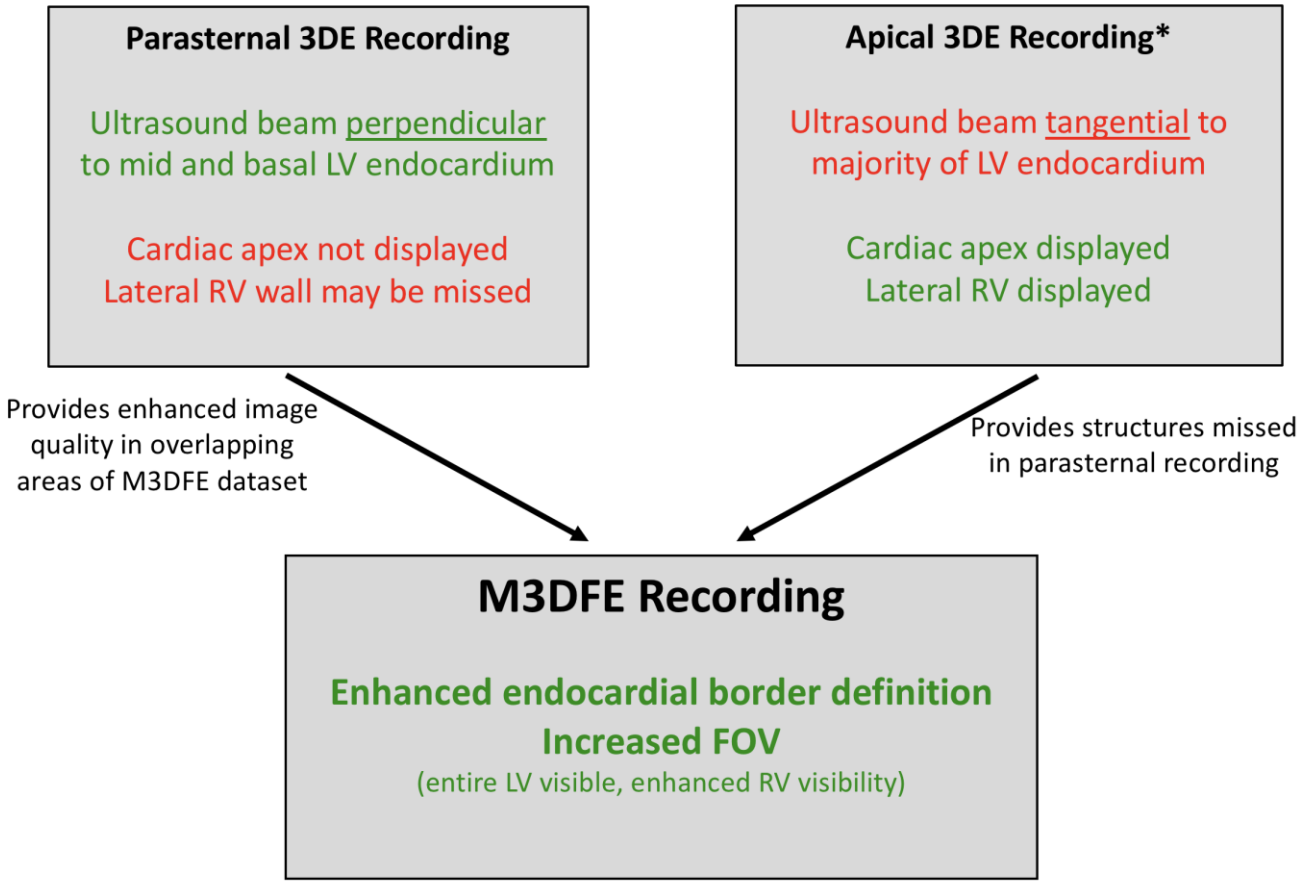

Chapter 1, Figure 4: Description of the mechanism of improved image quality by fusing parasternal and apical 3DE datasets. Red text = unfavorable/undesirable characteristic, green text = favorable/desired characteristic.

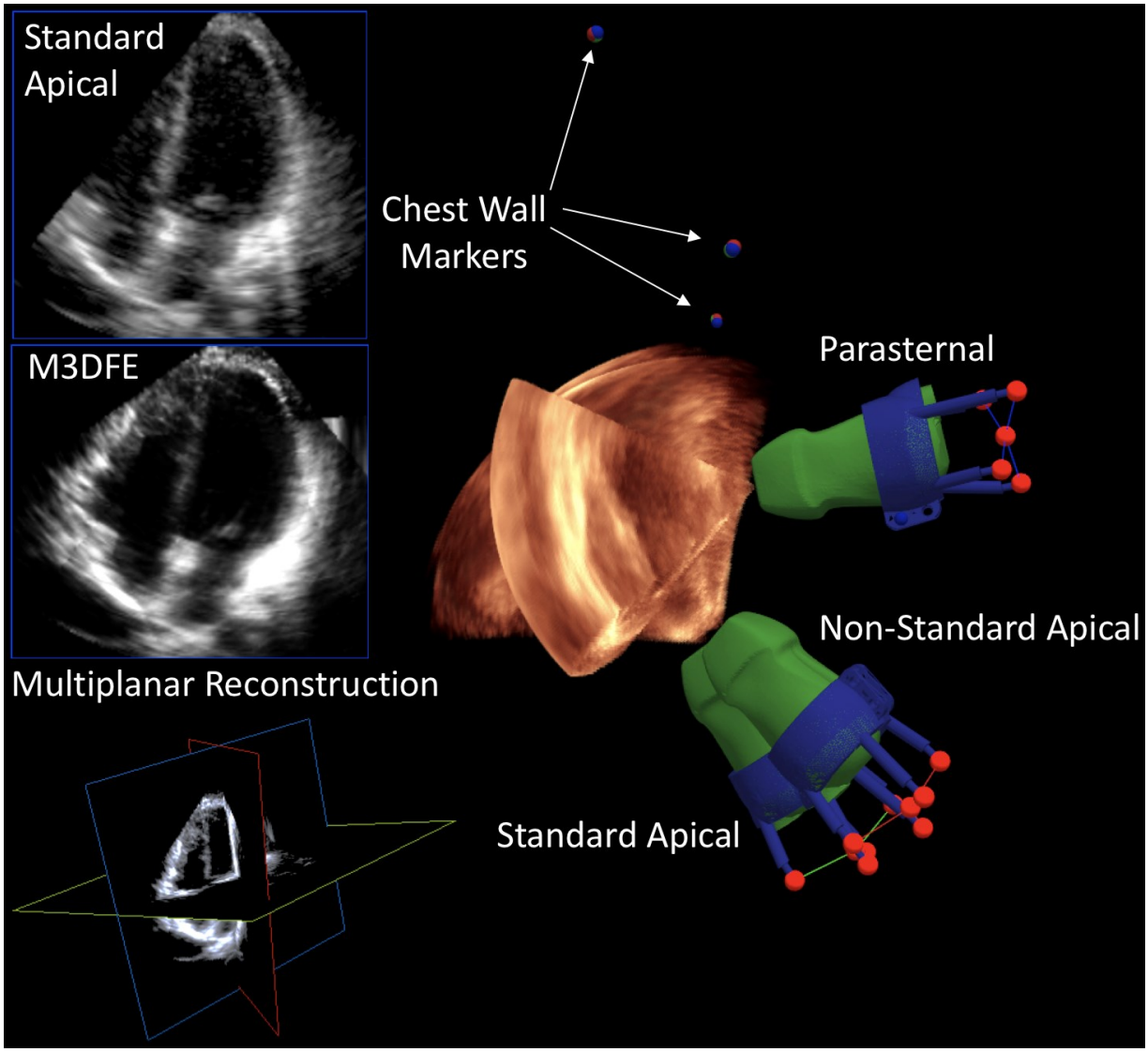

Chapter 1, Figure 5: A M3DFE dataset created using infrared optical tracking of both the transducers and chest markers. Left: 4-chamber views reconstructed from both standard apical 3DE and M3DFE datasets. Note the increased FOV and improved image quality (reduced LV cavity noise is prominent in this example). Right: The three transducer positions and corresponding 3DE volumes used to generate the M3DFE dataset (two apical and one parasternal in this case). Transducers are shown in green. Their corresponding mounts are shown in blue, and infrared reflective markers are in red. Each chest marker color corresponds to a transducer/3DE dataset with matching colored lines connecting the transducer markers.

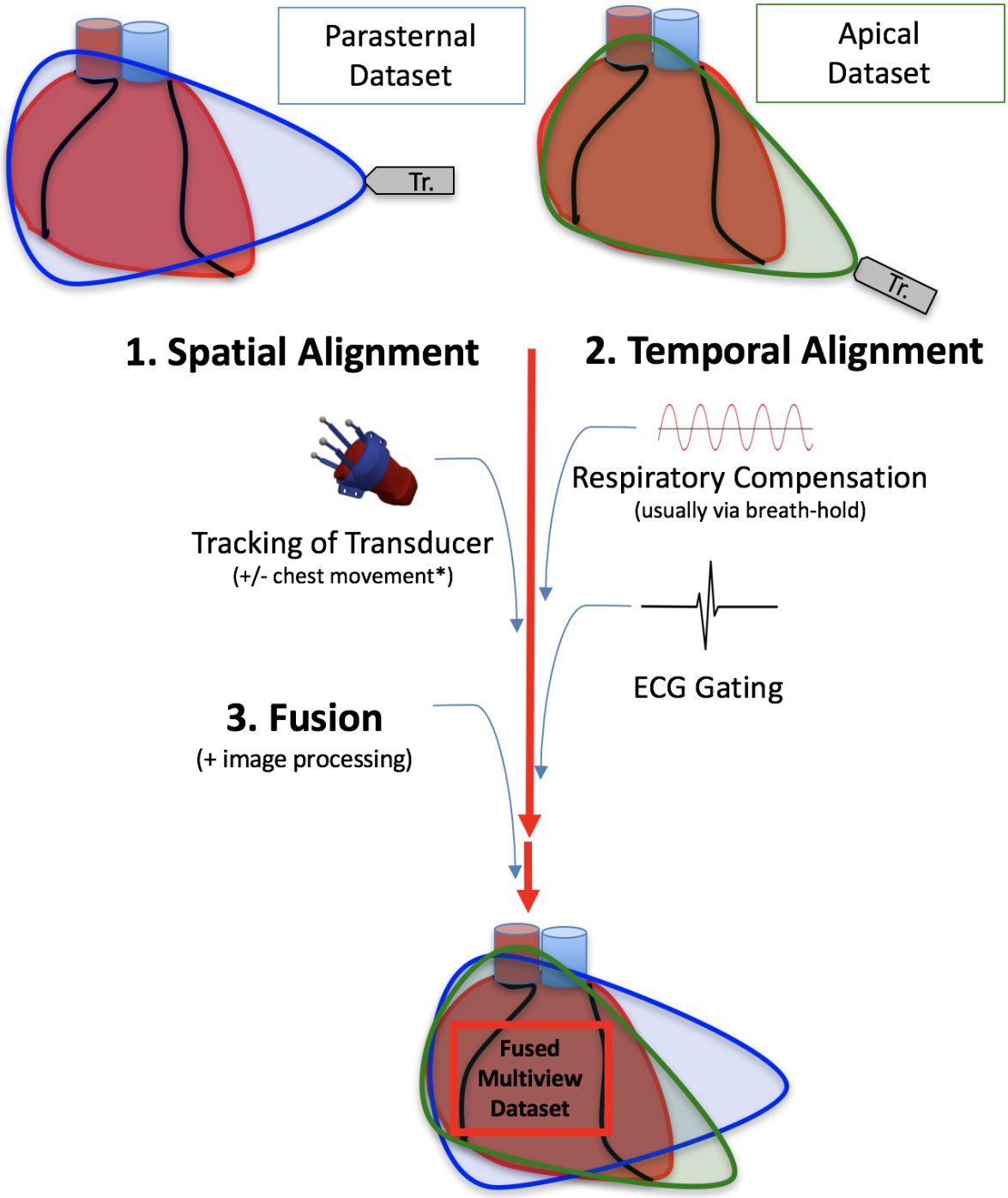

Chapter 1, Figure 6: Basic steps required to create a multi-view fusion echocardiogram. Tr = transducer. *Accounting for body/chest movement is an important step to ensure optimal spatial alignment.

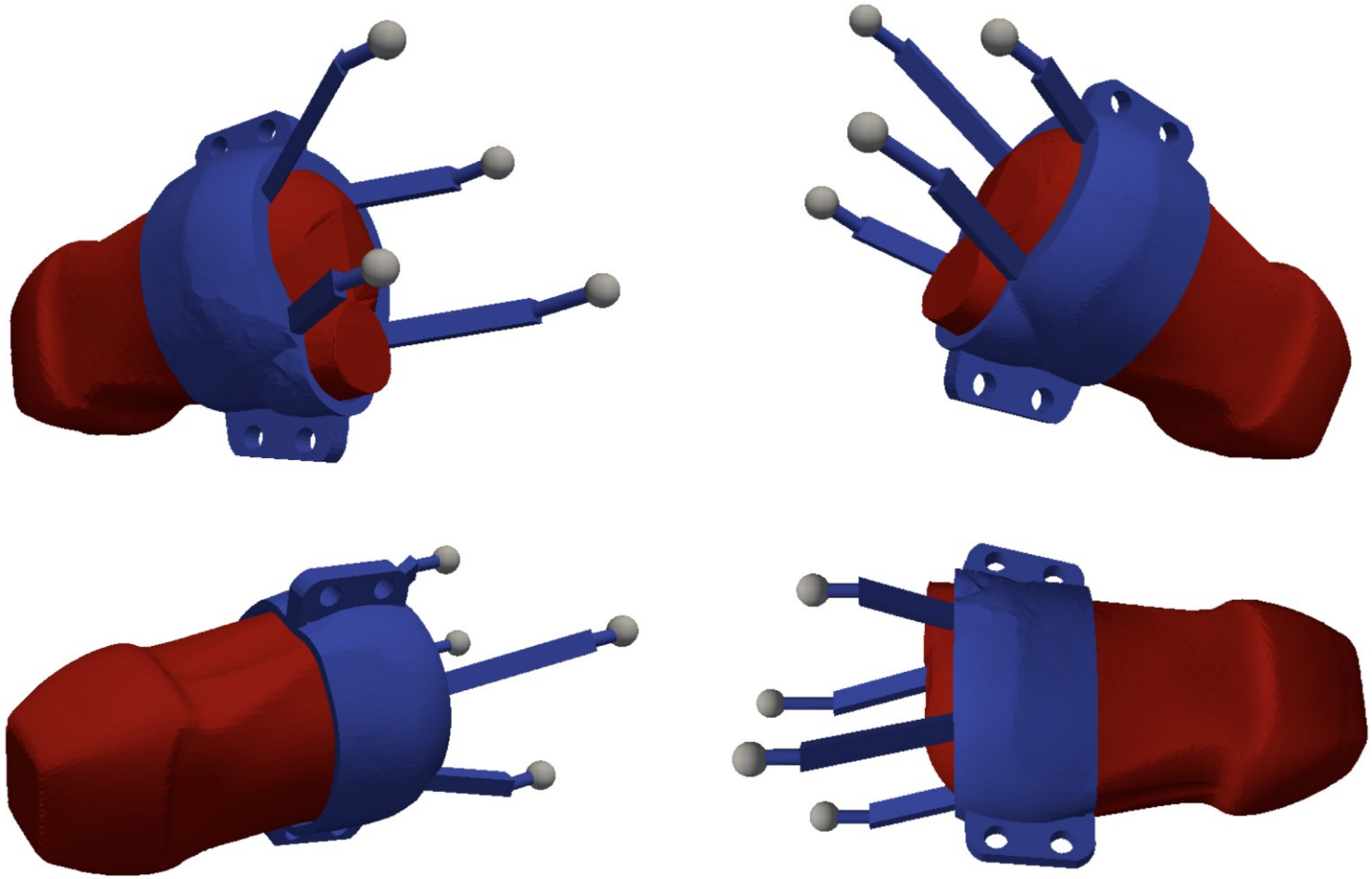

Chapter 1, Figure 7: 3D rendering of the transducer/marker apparatus created through laser scanning allows determination of the geometrical relationship between the optical markers and transducer footprint (and by extension, the recorded 3DE pyramidal volume). Multiple perspectives of the transducer are shown.

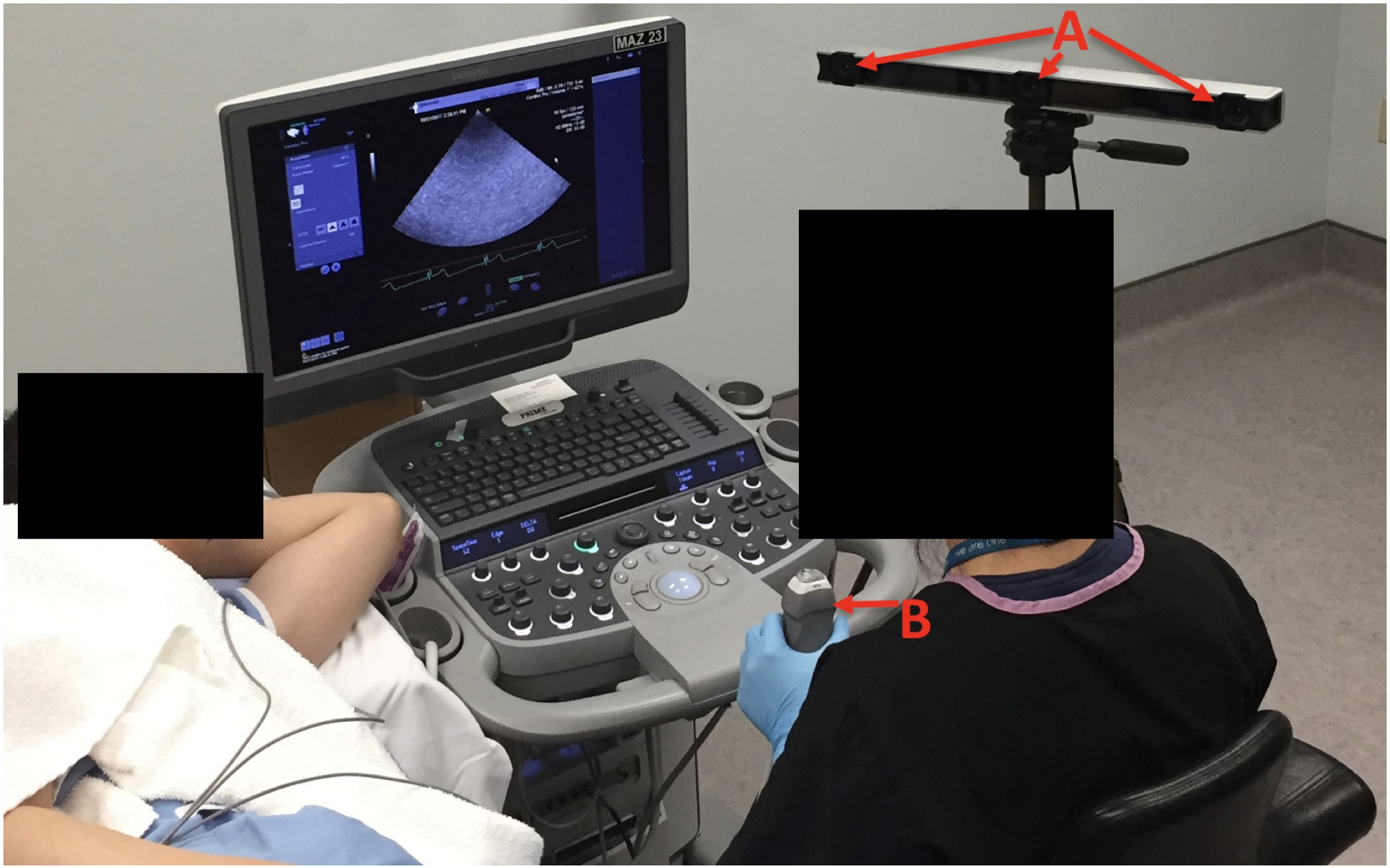

Chapter 1, Figure 8: Demonstration of the relationship between the sonographer, patient, ultrasound scanner and infrared optical cameras in a typical optical tracking setup. A = OptiTrack V120™ pre-calibrated infrared optical camera system mounted on a tripod. Red arrows point to each of the 3 individual cameras. B = Ultrasound transducer shown (markers are not seen from this angle).

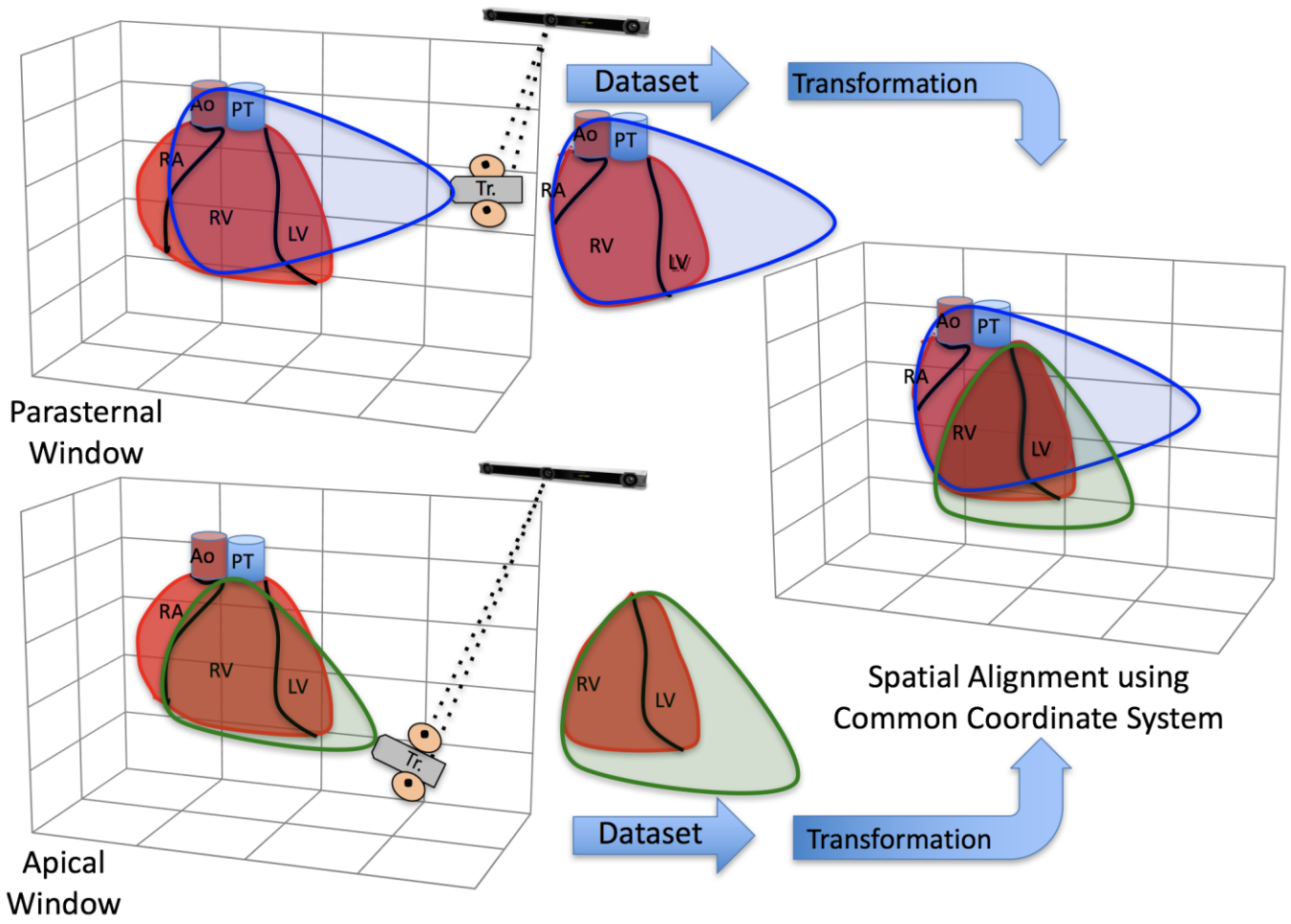

Chapter 1, Figure 9: M3DFE using optical transducer tracking. The optical tracking system documents the position and orientation of the transducers in three-dimensional space (an OptiTrack V120™ system is shown). The resulting ultrasound images are transformed onto a common coordinate system and subsequently fused. RA = Right Atrium, RV = Right Ventricle, LV = Left Ventricle, Ao = Aorta, PT = Pulmonary Trunk, Di = Diaphragm, Tr = Transducer with associated spherical optical markers.

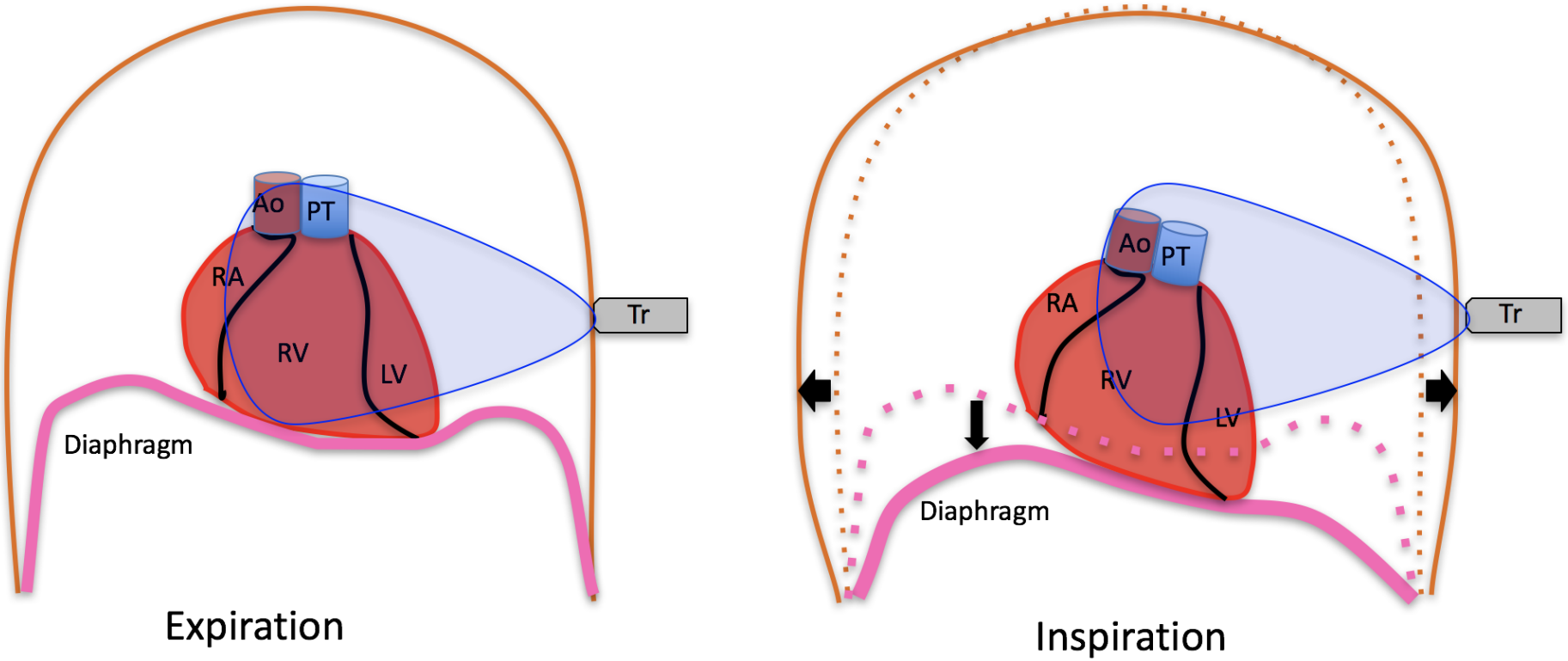

Chapter 1, Figure 10: Cardiac excursion resulting from respiration. Note the dynamic relationship between the heart and transducer throughout the respiratory cycle. RA = Right Atrium, RV = Right Ventricle, LV = Left Ventricle, Ao = Aorta, PT = Pulmonary Trunk, Tr = Transducer. Modified from Punithakumar et al.(20).

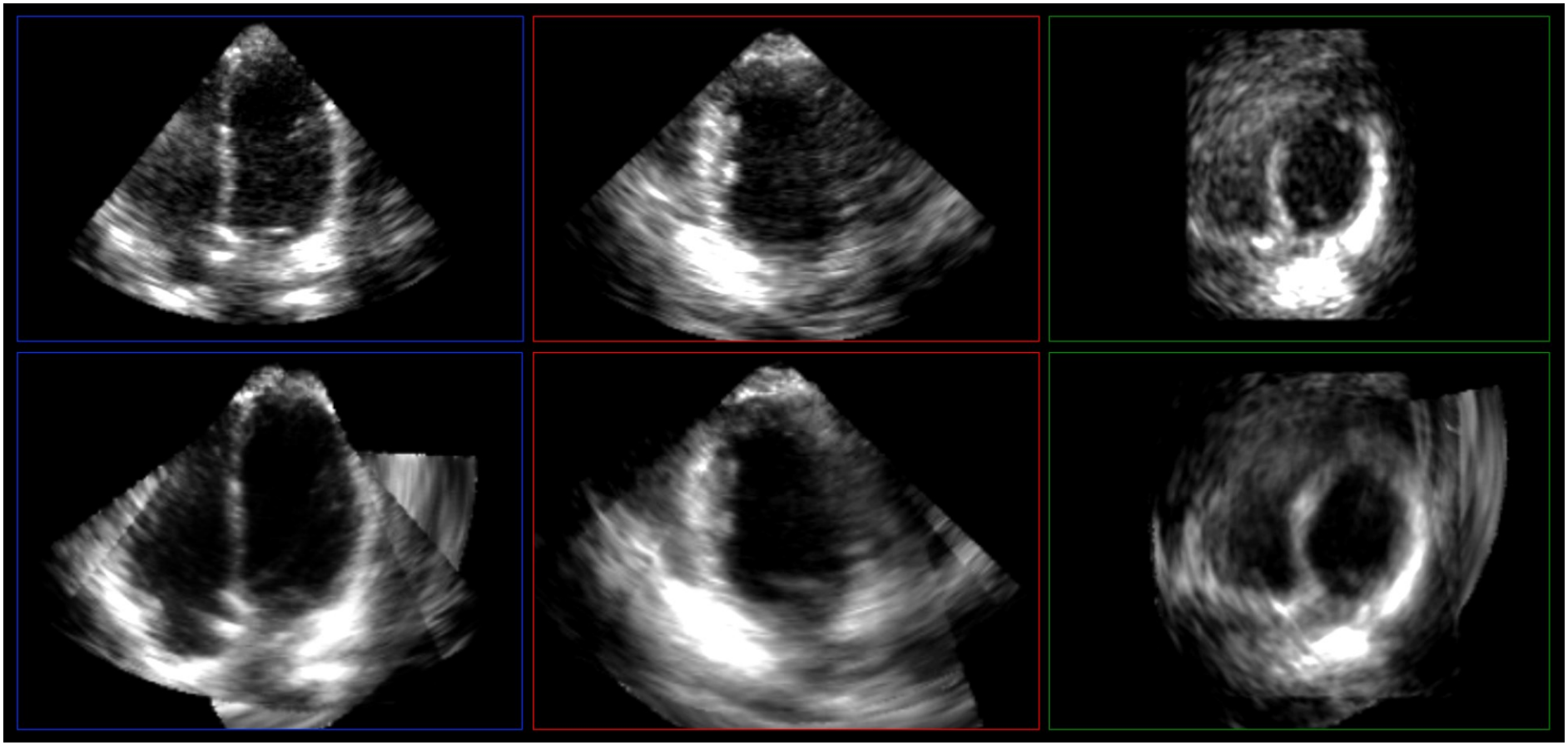

Chapter 1, Figure 11: Top row: Multi-planar reconstruction of a single apical 3DE volume. Bottom row: Multi-planar reconstruction of a M3DFE volume generated from fusion of the above single apical 3DE volume plus one additional non-standard apical 3DE volume and a parasternal 3DE volume (total of three contributing 3DE volumes). Note the increased FOV characterized by enhanced visibility of the lateral LV wall and RV. Also note the improved image quality with enhanced endocardial border definition and reduced noise in the LV cavity.

Chapter II

Multi-view Three-Dimensional Fusion Echocardiography Using a Novel Respiratory Tracking Technique: First Results in Humans

1. Introduction

1.1 Background – Important Limitations of 3DE

3-dimensional echocardiography (3DE) has been one of the greatest innovations in cardiac imaging to date and is currently the echocardiographic method of choice for quantification of left ventricular systolic function according to the American Society of Echocardiography (1). However, while developments in ultrasound transducer technology and post-processing techniques have undoubtedly bettered 3DE, they have failed to address inherent weaknesses of 3DE stemming from the nature of ultrasound physics. These include a limited field-of-view (FOV), reduced spatial and temporal resolution and reduced endocardial border definition (EBD) compared to 2-dimensional echocardiography (2DE).

In the context of echocardiography in general, poor EBD is largely explained by weakly reflected signals from important interfaces like the left ventricular (LV) endocardial border that often result from non-perpendicular, or tangential, angles of insonation. While angles of insonation approach perpendicular from the parasternal window, the entire chamber is not visualized from this perspective, necessitating the use of the apical window when performing chamber quantification. This is suboptimal since angles of insonation are non-perpendicular to the LV EBD when viewed from the perspective of the apical window (2). While this issue can be circumvented by using an alternative imaging modality such as cardiac magnetic resonance imaging, this modality does not offer a realistic replacement for echocardiography, which is by far the most commonly used cardiac imaging test owing to its low cost, versatility, portability and accessibility (3, 4). Echocardiographic contrast agents can improve endocardial border definition and LV volumetric analysis, but are expensive when used routinely, can be

time-consuming to administer, and still do not address the inherent limitation of tangential angles of insonation.

1.2 Multi-view 3D Fusion Echocardiography

A technique called 'multi-view 3D fusion echocardiography' (M3DFE) provides a solution to this dilemma by fusing partially redundant but complementary 3DE datasets from different acoustic windows. Multiple steps are required to generate high-quality M3DFE datasets (Figure 1). One of the most technically challenging aspects of M3DFE is achieving spatial alignment of individual datasets, that is, when each contributing 3DE volume is perfectly superimposed on the next. Achieving this goal is critical to the success of M3DFE – even subtle misalignment can result in contour blurring that would render the dataset unsuitable for diagnostic purposes.

Numerous studies, the majority of which have been pre-clinical, have examined various M3DFE protocols. These studies have demonstrated improvements in parameters such as field-of-view (FOV), EBD, contrast, contrast-to-noise ratio (CNR), signal-to-noise ratio (SNR), and perception of imaging artifacts (2, 3, 5-18). Despite these promising findings, however, two important challenges exist: i) no clinically feasible alignment protocol exists, and ii) there is no consensus on the optimal way to process overlapping portions of M3DFE datasets. The purpose of this study, therefore, is to enhance the feasibility and effectiveness of M3DFE by creating a protocol which is conducive to further investigation in clinical settings. This will be accomplished through two mechanisms. First, through the development of a new tool which aids in the optimization of spatial alignment. Second, through comparing two methods of 3DE fusion to ascertain which is the preferred approach.

1.3 Hypotheses

Hypothesis #1:

In an effort to enhance the accuracy and efficiency of spatial alignment, we developed a novel screening procedure which can predict which M3DFE datasets will, or will not, demonstrate adequate alignment. This approach has the ability to prevent time-consuming image processing and analysis of poor datasets, and can aid in the preferential selection of

only the highest quality datasets for further analysis. It involves a quantitative screening procedure which helps to determine whether healthy volunteers were able to remain still and perform an adequate breath-hold during the recording of successive 3DE datasets planned for fusion. We hypothesize that >90% of M3DFE datasets passing the screening test will be of sufficient quality for diagnostic use, as validated by a subjective assessment by two echocardiographers whereby neither is able to detect any evidence of subjective misalignment.

Hypothesis #2:

We also evaluate a fusion technique called 'fusion by wavelet decomposition', which has shown promising results in prior works (7, 16). We hypothesize this method will yield superior improvements in subjective and objective measures of image quality as compared to a more basic technique, 'fusion by voxel averaging' (note that a 'voxel' is the 3-dimensional (3D) equivalent of the 2-dimensional (2D) 'pixel'). If fusion by wavelet decomposition is, in fact, superior to fusion by voxel averaging, future investigators can consider its application when performing clinical studies in those with cardiac disease, and when validating results of volumetric analysis using M3DFE compared to contrast echocardiography and/or cardiac magnetic resonance imaging.

2. Methods

2.1 Subject Enrollment

Approval to undertake this study was granted from the University of Alberta Research Ethics Office, and allowed for enrollment of up to 12 healthy adult volunteers (Study ID: Pro00057214). Volunteers were recruited via an advertisement posted to an online forum frequented by University of Alberta medical students. Any healthy adult without a personal history of cardiac disease was eligible to participate. Participants provided written informed consent prior to each session. There was no financial incentive to participate, but any travel costs were payed for by our research laboratory. Basic demographic information of each participant was recorded (age, gender, weight and height).

2.2 Equipment and Materials

All studies were performed by an experienced sonographer at the Alberta Cardiovascular and Stroke Research Centre at the University of Alberta. Real-time 3DE recordings were acquired using a Siemens Acuson SC2000 scanner and 4Z1c matrix array transducer.

Three infrared cameras (OptiTrack V120, USA) mounted on a tripod were used to track the 3-dimensional (3D) position and orientation of the transducer and chest markers (Figures 2-4). Ultrasound transducer and chest marker tracking was monitored and displayed in real-time on a 3D display using a nearby computer workstation. This computer workstation also served as a hub to which all information was directed and stored for later off-line processing.

2.3 Data Recording

3DE recordings were obtained during a breath-hold maneuver using 3 separate imaging protocols: i) an unmoving transducer capturing single standard apical volumes (UNM imaging protocol), ii) a moving transducer capturing standard plus non-standard apical volumes resulting from slight changes in probe angulation and/or 1-2cm medial-lateral movements of the transducer (NSA imaging protocol), and iii) a moving transducer with the probe positioned to capture both standard (+/- non-standard) apical volume(s) plus a parasternal volume (AP imaging protocol). Electrocardiographic information was collected and stored in association with each echocardiographic recording.

Optical tracking data was collected and stored in a separate file corresponding to its matching 3DE recording. If the optical tracking system failed to maintain its detection of the transducer or chest marker positions at any time during a 3DE recording, that 3DE recording, as well as its counterparts that were planned to comprise its M3DFE dataset, were discarded. Loss of detection was usually the result of an unintended obstruction in the line-of-sight between the cameras and the transducer/chest markers.

A range of 2-5 real-time, single cardiac cycle 3DE recordings were obtained per breath-hold for each of the above three protocols. Breath-holds were generally performed at end-inspiration or end-expiration depending on which yielded better images. The number of

recordings per M3DFE dataset depended on the length of time the subject could maintain a breath-hold maneuver.

Variable sector depths, dimensions and line densities were used when switching between the apical and parasternal windows for a given M3DFE dataset. This was necessary to achieve two goals: i) to *maximize* the volume-rate (temporal resolution) while ensuring the sound-field was large enough to adequately visualize the variably sized left ventricles, and ii) to ensure a *stable* volume-rate between the apical and parasternal recordings. In order to achieve successful temporal alignment, each recording contributing to the M3DFE dataset must be recorded at a relatively similar heart rate and contain a relatively similar number of volumes. Using this strategy, volume-rates ranged between 21-24 volumes/second.

Recordings from apical windows were obtained using fundamental frequency imaging at 2.8MHz; recordings from the parasternal window were obtained using harmonic frequency imaging, also at 2.8MHz. The decision to choose fundamental frequency imaging for apical windows was based on our goal of optimizing image quality in the near-field, as fundamental frequency imaging yields greater signal strengths than harmonic imaging at very shallow imaging depths (19). In addition, near-field clutter artifacts were much more prominent when using harmonic imaging (an example is shown in Figure 2). By optimizing the near-field from the apical window using fundamental imaging (apical LV segments), and optimizing deeper imaging from the parasternal window using harmonic imaging (mid and basal LV segments), we aimed to generate M3DFE volumes demonstrating LV's with superior image quality compared to what could be achieved using the apical window alone (20).

2.4 Creation of M3DFE Volumes

In order to process and manipulate the 3DE data, a Microsoft Windows®-based customized 3DE software program was created. The minimum computer specifications required to run this program efficiently are as follows: Microsoft Windows 7® operating system, a 3.60 GHz Core™ i7 processor and 64GB RAM.

The program enabled us to create M3DFE datasets by automatically spatially aligning 3DE recordings corresponding to each M3DFE dataset. Temporal alignment was by ECG-gating, with each cine-loop being set to begin with the 3DE volume corresponding to the onset of the QRS complex as detected by the ECG.

If contributing 3DE recordings were of variable durations, as measured by the number of volumes per recording, the longer 3DE recording(s) were truncated to match the number of volumes of the shortest 3DE recording. For example, if a M3DFE dataset was comprised of two 3DE recordings – one consisting of 22 volumes and the other consisting of 21 volumes, the first recording would be truncated to contain 21 volumes. Any subtracted volumes were taken from the tail-end of the recording, at end-diastole, as the heart moves least during this phase of the cardiac cycle and this strategy therefore is expected to minimize any impact on assessments of cardiac motion.

2.5 Manipulation of M3DFE Volumes

Once a desired selection of 3DE recordings is loaded by the viewer to create a M3DFE volume, the user is able to manipulate this volume using a number of functions. These include: i) toggling individual 3DE volumes on/off, ii) multi-planar reconstruction (MPR) of the M3DFE volume to produce three different 2D planes, iii) magnification of the 2D planes, iv) toggling between a multi-plane view and a full-screen view of a particular 2D plane of interest, v) visualization of the transducer(s) and chest markers in relationship to the M3DFE volume, vi) analysis of contrast, CNR and SNR by placement of two region-of-interest (ROI) boxes (one myocardial box and one LV cavity box), vii) adjustment of brightness and contrast levels, ix) toggling between fusion by voxel averaging and wavelet decomposition, x) display of the FOV and number of volumes per cine loop, xi) display of the mean chest marker displacement, xii) play/pause of cine loop with the ability to move forward/backward one volume at a time when the loop is paused, xiii) ability to save the M3DFE volume, including any manipulations to the MPR (for future assessment and in order to create a library of M3DFE examples) and xiv) the ability to save a video recording of the cine-loop for future demonstration (.avi format). Figure 7 displays a screenshot of the viewer.

2.6 Screening for Spatial Alignment

Before proceeding with MPR and further analysis, we performed a novel screening procedure to ensure each M3DFE volume was adequately aligned. We believed this procedure would enhance the probability of producing optimally aligned M3DFE datasets, and

consisted of a quantitative assessment of mean chest marker displacement. For the quantitative assessment, chest marker tracking data was used to determine the mean chest marker displacement. This computation was performed and displayed automatically by the software viewer. Here, the mean difference in chest marker displacement, *D*, between individual 3DE recordings was computed as follows:

$$D = \left[\frac{1}{N(N-1)} \sum_{i=1}^{N} \sum_{j=1}^{N} d_{ij} \right]$$

$$d_{ij} = \begin{cases} 0 \;\; if \;\; i = j \\ \frac{1}{M} \sum_{k=1}^{M} \left\| m_k^i - m_k^j \right\| \;\; otherwise \end{cases}$$

Where *N* denotes the number of 3DE recordings, *d* denotes the average distance for each pair of 3DE recordings, *M* denotes the number of chest markers and *m* denotes the position of each chest marker. The operator || represents the Euclidian distance between the corresponding markers in 3-dimensional space. In essence, *D* is the average distance between all possible combinations of corresponding chest markers.

If the mean displacement between chest markers exceeded a threshold of 1.5mm for a given M3DFE dataset, results were discarded as this indicated a failed breath-hold maneuver or subject movement during the recording and therefore predicted a poorly aligned, and thus suboptimal, M3DFE result (Figure 8). The threshold of 1.5mm was chosen because it is between the 1mm axial and 2mm lateral resolutions which typically characterize real-time 3DE systems (21).

In order to test our hypothesis that >90% of studies passing the above screening procedure would result in spatially aligned datasets suitable for diagnostic assessment, two echocardiographers (TL + HB) viewed each study passing the quantitative screen to validate whether or not they perceived any misalignment.

2.7 Fusion Methods

When individual 3DE volumes are combined to create a M3DFE volume, data existing in the region of overlap must be combined or 'fused' to generate an image. A number of fusion techniques have been previously studied, each processing overlapping information differently to yield different results. We chose to assess two such methods in this study. The first is a basic approach called fusion by 'voxel averaging', which will henceforth be referred to as 'AVG'. The second, more sophisticated approach called fusion by 'wavelet decomposition', which will henceforth be referred to as 'WAV', was chosen because it has demonstrated promising results in prior studies (7, 16). Given there is no current consensus on an optimal fusion technique, we wished to determine whether we could reproduce these results to generate M3DFE datasets of superior quality to those generated by the AVG technique.

2.7.1 Fusion by Voxel Averaging

When applying this technique, the final display of overlapping regions is generated using the mean voxel intensity of corresponding voxels from each contributing 3DE volume. This method is effective at reducing noise since it occurs at random and therefore should be diminished by the averaging process. However, a major weakness of the AVG method is that if one contributing volume shows a favorable/strong signal in a particular myocardial segment, but the other shows an unfavorable/weak signal in the same region, the favorable signal is attenuated since it is averaged with the weak signal. In this scenario, the appearance of the negatively affected region may actually be worse on the M3DFE volume than on the single best individual 3DE volume. Another weakness is the appearance of 'stitching-like' artifacts on the M3DFE volume characterized by clearly visible boundaries separating overlapping individual volumes (7).

2.7.2 Fusion by Wavelet Decomposition

Fusion using WAV is based on an image processing technique which separates overlapping portions of M3DFE volumes into low- and high- frequency components then differentially processes these components to generate a fused image. An in-depth description of the specifics of WAV is beyond the scope of this manuscript but can be found elsewhere (7).

Essentially, the WAV algorithm works to enhance the appearance of low-frequency components relative to high-frequency components. Since high-frequency components are thought to generally consist of noise and artifacts, and low-frequency components are generally thought to consist of 'true' signals of interest (resulting from structures such as the myocardium), the result is an improvement in subjective image quality, contrast, CNR and SNR compared to basic techniques like AVG (7, 16).

2.8 Study Design

As mentioned in section 2.3, three imaging protocols were used to collect data from each subject. One M3DFE volume produced using each of the three imaging protocols was analyzed per subject. Therefore, a total of three M3DFE volumes were analyzed per subject. Multiple successful M3DFE datasets were usually generated for each subject's three imaging protocols. The M3DFE volume containing the subjectively most favourable standard apical 3DE volume (non-fused) was chosen for analysis. This approach was used to avoid biasing results to favour the M3DFE groups, and because standard clinical practice uses non-fused standard apical 3DE volumes to perform LV quantification.

Using the software viewer, MPR of the M3DFE volume was then performed to generate 4- and 2- chamber 2D planes. MPR was performed to maximize LV volume / minimize LV foreshortening. Since the non-fused standard apical 3DE volume was always one of the contributing volumes in a given M3DFE volume, both volumes were subjected to an identical MPR. MPR therefore generated identical 2D planes for both individual 3DE and M3DFE volumes.

MPR was performed in this manner for both end-diastolic and end-systolic volumes. The rationale for studying both phases of the cardiac cycle related to our belief that results during systole and diastole should be proven consistent given the implications for future validation studies assessing M3DFE's accuracy in LV volumetric analysis.

Reconstructed 2D planes were subjected to both subjective and objective analyses of each of the 6 standard ASE myocardial segments for both 4- and 2-chamber planes (= 12 segments analyzed per 3DE volume). All 12 segments were then analyzed within the following three imaging *groups* (note the distinction from the three imaging *protocols*): i) the non-fused, single standard apical 3DE volume (control/comparator group, henceforth known as the SSA

group), ii) a M3DFE volume generated using fusion by the AVG method and iii) a M3DFE volume generated using fusion by the WAV method. For each M3DFE dataset, this analysis yielded a maximum of 36 visualized segments for each of end-diastole and end-systole, or a maximum of 72 segments. Since this was performed for each of the three major imaging protocols described above, a maximum of 216 segments were visualized per subject. A flow diagram illustrating the study design is shown (Figure 9).

2.9 Data Analysis:

Objective assessments of image quality consisted of an evaluation of the following parameters: i) contrast, ii) CNR, iii) SNR and iv) $\triangle$FOV (% increase in FOV). Subjective assessments included i) successful alignment of datasets – either aligned or not aligned as assessed by two echocardiographers (TL +HB), with datasets appearing even slightly misaligned by either observer being excluded and ii) an evaluation of EBD. EBD was evaluated according to a three-level scale from 0 to 2, with 0 = not visible, 1 = poorly defined and 2 = clearly defined.

Endocardial border definition, contrast, CNR and SNR were assessed on a per-myocardial segment basis for each of the standard myocardial segments described above. This analysis was performed by a single echocardiographer (TL). Contrast, CNR and SNR values were derived from the mean and standard deviation of pixel intensity values of two region-of-interest (ROI) boxes. One ROI box was placed in the myocardium; the other was placed in the adjacent LV cavity. Specifically, ROI boxes were positioned using the non-fused SSA volume. The myocardial ROI box was placed at the position of the greatest/optimal signal within the compact myocardium of each LV segment, and the LV cavity box was placed in the adjacent blood pool just beyond any visible trabeculations. With both ROI boxes remaining in stable positions, the two different fusion algorithms were successively applied to generate new contrast, CNR and SNR values which were then recorded (Figure 11).

Segments that were not subject to the effects of volume overlap and fusion (eg. apical segments in the AP group), and segments that were not visible (eg. due to near-field clutter, signal dropout or acoustic shadow) were excluded from the analysis.

2.10 Computation of Objective Parameters:

The mathematical equations for each objective parameter along with their corresponding descriptions are seen below. In the spirit of maintaining stable conditions between datasets, brightness and contrast were not manually adjusted given the effect on pixel intensity values which might result in altered contrast, CNR, SNR and EBD data.

Contrast is computed as follows: (7, 22)

$$Contrast = \mu^{MY} - \mu^{BP}$$

Here, μ^{MY} is the mean pixel intensity in the manually selected region of interest in the myocardium; μ^{BP} is the mean pixel intensity in the manually selected region of interest in the adjacent left ventricular cavity / blood pool.

CNR is computed as follows: (22, 23)

$$CNR = \frac{\mu^{MY} - \mu^{BP}}{\sigma^{BP}}$$

Here, μ^{MY}, μ^{BP} are as described above. σ^{BP} refers to the standard deviation of the pixel intensity within the region of interest box placed in the LV cavity / blood pool adjacent to the corresponding myocardial ROI box. Since a perfect image demonstrates an absence of signal (completely black LV cavity / blood pool), the standard deviation of any signal here is considered to be noise (22, 23). Note that since the myocardium has a natural variation, or 'texture', in signal intensity owing to inherent tissue characteristics, σ^{MY} was not considered as reflecting 'noise' but rather an expected and phenomenon of myocardial imaging.

SNR is computed as follows: (22, 24)

$$SNR = \frac{\mu^{MY}}{\sigma^{BP}}$$

Here, μ^{MY} and σ^{BP} are as described above. Since the desired 'signal' of interest is the myocardial signal, the numerator is μ^{MY}.

ΔFOV is computed as follows:

$$\Delta FOV = \left[\frac{FOV_f}{\frac{1}{N}\sum_{i=1}^{N} FOV_i} - 1\right] \times 100$$

where FOV is defined as:

$$FOV = \sum_{v=1}^{n} d(v), \text{ where } d(v) = \begin{cases} 1, \text{ foreground} \\ 0, \text{ background} \end{cases}$$

Variable v denotes the v^{th} voxel in the echocardiographic scan. The foreground was taken as the voxels with non-zero intensity values and the background was taken as the voxels with zero intensity values. FOV_f refers to the field- or 'volume'-of-view of the M3DFE volume; FOV_i refers to the volume-of-view of individual contributing 3DE volumes.

In essence, the ΔFOV is the % increase in the 'volume'-of-view as seen with the M3DFE volume (the numerator) as compared to the average 'volume'-of-view of all individual contributing 3DE volumes (which is the reference for comparison, or denominator).

2.11 Statistical Analysis Comparing SSA vs AVG vs WAV:

Since multiple groups were to be compared a randomized block design analysis of variance (ANOVA) test was chosen for the analysis. The null hypothesis was defined as follows: there is no difference in image quality between any of the groups (SSA and either M3DFE by AVG or WAV, or between M3DFE by AVG vs. M3DFE by WAV), as assessed using the parameters of contrast, CNR, SNR and EBD.

The alpha statistic was set at 0.05 and the beta statistic at 0.80. Given we aimed to demonstrate superiority in our comparisons, a one-tailed test was used. Although we expected AVG to be inferior to WAV in terms of contrast measurements, this relationship is already known. We therefore felt it would be unwise to 'waste' statistical power by splitting the test into two-tails only to confirm what is already known (7).

Since multiple analyses were conducted, a Tukey Honest Significant Difference (HSD) correction was performed to reduce the risk of a type I error ('false positive'). The Tukey HSD

test was chosen because it tends to sacrifice less statistical power than others such as the Bonferroni correction, as were already concerned that our small sample size may result in less-than-ideal statistical power and resultant type II errors ('false negatives').

2.12 Inter-rater Agreement Analysis:

An inter-rater agreement analysis was performed to assess the reproducibility of our method. Two echocardiographers (TL + HB) rated EBD and collected mean and standard deviations of pixel intensities from ROI boxes from a small sample of 3DE volumes in the same fashion as described in section 2.7 above. One representative M3DFE dataset was chosen for each imaging protocol and was then subjected to analysis on the end-diastolic volume as chosen by each observer. This resulted in the generation of contrast, CNR, SNR and EBD values for a total of 108 myocardial segments across 3 M3DFE datasets. Inter-rater agreement was assessed by calculating an intra-class correlation coefficient for continuous variables (contrast, CNR, SNR), and weighted Kappa statistic for the categorical variable (EBD)(25-28).

3. Results

3.1 Study Subjects

A total of 12 healthy adult volunteers with no history of cardiovascular disease participated in the study, but data from the first volunteer were discarded due to a technical issue with the software viewer's handling of optical tracking data. Consequently, data from 11 volunteers was analyzed. Eight were male (73%) and 3 were female (27%). The mean ± standard deviation of age was 24.5 ± 2.7years, of weight was 73 ± 19kg and of height was 174 ± 9cm. A total of 1,686 segments were analyzed to generate values for contrast, CNR, SNR and EBD. The data acquisition process lasted approximately 30 minutes per subject.

3.2 Validation of Quantitative Screening Procedure

A total of 148 attempts at creating M3DFE datasets were made. Of these, 75 (51%) maintained optical tracking of the transducer and chest markers for the duration of each

contributing 3DE recording. These datasets were eligible for the quantitative screening procedure. Of the 75 M3DFE datasets screened, 65 (87%) 'passed' the screen with mean chest marker distances <1.5mm. Of the 65 datasets 'passing' the screen 63 (97%) were validated as 'suitable for diagnostic assessment' as judged by two echocardiographers who both agreed these 63 cases showed no signs of subjective misalignment. This translates into 63/148 (43%) total attempts yielding a diagnostically suitable M3DFE dataset, and also confirms our hypothesis that >90% (97%) of M3DFE datasets passing this novel quantitative screening test would yield M3DFE datasets suitable for diagnostic use.

Of the M3DFE datasets selected for analysis, the mean chest marker distance was 0.28mm ± 0.29mm (range 0.1mm – 1.4mm). Save one exception, at least one successful dataset was generated for each of the three imaging protocols for all eleven volunteers. The exception was noted in a subject who had great difficulty cooperating with breath-hold maneuvers, leading to M3DFE datasets with mean chest marker distances consistently >>1.5mm for the AP imaging protocol. This particularly prominent example of misalignment is shown in Figure 10.

3.3 Endocardial Border Definition

Fusion by AVG consistently improved EBD in the UNM protocol (2/2 cases), inconsistently in the NSA protocol (1/2 cases) and never in the AP protocol (0/2 cases). Fusion by WAV consistently improved EBD for all protocols (6/6 cases). When directly comparing the two M3DFE methods, WAV was shown to be superior to AVG in 4/6 cases. Raw data for end-systole and end-diastole are seen in Figures 1 and 2 respectively; results of the ANOVA test + Tukey HSD correction for end-systole and end-diastole are shown in Tables 3 and 4 respectively.

3.4 Objective Evaluation of M3DFE Datasets

As had been shown previously, contrast was consistently reduced using AVG, but was recovered following the application of WAV as exemplified in Figure 11 (7). WAV was consistently superior to AVG for contrast measurements, except for in the NSA group during systole (5/6 cases). Fusion by both methods consistently improved both the CNR and SNR,

except for in the AP group during systole. WAV never showed superiority to voxel averaging in CNR measurements, but demonstrated superiority in SNR in the AP group in both systole and diastole. Raw data for end-systole and end-diastole are seen in Figures 1 and 2 respectively; results of the ANOVA test + Tukey HSD correction for end-systole and end-diastole are shown in Tables 3 and 4 respectively.

3.5 Field-of-view

ΔFOV was enhanced in all three imaging protocols. Specifically, ΔFOV was +11% ± 5% for the UNM protocol, +33% ± 25% for the moving transducer with NSA view(s) protocol, and +47% ± 12% for the moving transducer with the AP protocol. The increase in ΔFOV seen in the UNM transducer group is attributed to slight unintentional movements of the transducer during acquisition of successive 3DE recordings. The much greater improvements seen in the NSA group and AP group are attributed to the correspondingly greater movements of the transducer which allowed enhanced cardiac visualization.

3.6 Inter-rater Agreement Analysis

Results of the inter-rater agreement analysis are shown in table 5. Good agreement was noted for contrast, poor agreement was noted for SNR and moderate agreement was noted for CNR and EBD. Suboptimal results likely reflect two factors. First, the relatively small sample that was assessed by each observer (108 segments). Second, the relatively small ROI boxes used during data collection, as only a small section of each myocardial segment and adjacent LV cavity was selected by each observer. In the future, we plan to enhance the inter-rater agreement by updating the software viewer to allow users to select ROI's by manually tracing the entire segment and adjacent LV cavity.

4. Discussion

4.1 Addressing Two Major Challenges Facing M3DFE

To our knowledge, this is the first study in humans to utilize a quantitative respiratory tracking technique to guide spatial alignment in M3DFE. Results of this study confirm both of our hypotheses and represent significant breakthroughs in addressing two major challenges facing M3DFE. First, we confirmed our hypothesis that >90% of M3DFE datasets passing the screen would be suitable for diagnostic assessment (97% in this study). This suggests that our novel quantitative respiratory tracking technique provides an effective strategy which ensures that only recordings for which patients remained still and maintained an adequate breath-hold are used for fusion. This approach to predicting adequate spatial alignment of M3DFE datasets, a step we believe is critical in the optimization of M3DFE datasets, represents a significant step forward in the clinical feasibility of M3DFE.

Second, results are generally supportive of our hypothesis that fusion by WAV is superior to fusion by AVG – an important finding given the many possible ways to perform fusion and the lack of clear consensus as to which method yields superior results. It is noteworthy that WAV performs especially well during AP fusion. The added benefits of WAV in AP fusion are not surprising. Often, favorable interventricular septal signals in the SSA group were attenuated when the AVG method was applied to perform fusion with a parasternal volume containing weak interventricular septal signals. Following the application of WAV, however, these attenuated signals were almost always completely recovered.

4.2 Comparison of Imaging Protocols

The ΔFOV was progressively enhanced from the UNM → NSA → AP imaging protocols as expected. However, an unexpected finding was that the magnitude of benefit to image quality did not appear greatest with the AP protocol. While the three imaging protocols were not formally compared, the relatively similar magnitude of benefit between protocols is clearly seen from examining the '% difference in means' in Tables 3 and 4. While it was encouraging to note that significant benefits were achieved even with an unmoving transducer, we expected a similar step-wise improvement in image quality from UNM → NSA → AP protocols given the progressive diversity in angles of insonation.

One explanation is that, given participants were young healthy volunteers with ideal acoustic access, and apical windows were favorable even before fusion, there was often little to gain by adding a parasternal view. This is in contrast to what would be expected from

individuals with poor apical windows, where contribution from the parasternal window could add a significant benefit to the M3DFE volume. This gives credence to the notion that an 'ideal' subject for AP M3DFE is one in whom apical windows are particularly difficult and parasternal windows are particularly favorable. Such a patient is encountered relatively commonly in clinical practice. A future study comparing similar imaging protocols, but in patients known to have poor apical windows, would be helpful to provide further insight into which patient subsets might benefit most from AP M3DFE.

4.3 Limitations

There are important limitations to our study. First, our study is limited by a small sample size. However, because of the nature of our study design, this was mitigated by the large number of total segments analyzed (1,686). Second, only 43% of total attempts yielded a M3DFE dataset fit for diagnostic assessment. This was usually due to a loss in optical tracking signals. This issue could be addressed by introducing a second OptiTrack™ system which is strategically positioned to reduce the chance of losing line-of-sight with chest or transducer markers. Notwithstanding, the protocol was highly effective, with 97% of datasets passing the quantitative screen were fit for diagnostic assessment. Third, participants were healthy and had no history of cardiovascular disease. Results may therefore not be generalizable to a typical clinical population. However, we believe the benefits of M3DFE may be even more apparent in clinical settings where patients have cardiac disease and may be challenging to scan, since there may be relatively less to gain in young healthy volunteers in whom conventional 3DE already provides such excellent results. Fourth and perhaps most important was that it was not possible for us to demonstrate that the improvements in image quality translate into mirrored improvements in the accuracy of LV quantification. This was due to the fact that our software viewer is not currently capable of performing LV quantification, and datasets were not created in a format which could be loaded and manipulated by commercially available software packages. We expect that LV quantification measurements would demonstrate reduced variability and enhanced accuracy compared to accepted techniques such as contrast echocardiography or cardiac magnetic resonance, but this hypothesis will require further validation in future studies.

4.4 Future Directions

There are many potential ways to deploy real-time M3DFE in order to maximize the potential of echocardiography. It has previously been shown that progressively greater results are seen as progressively more datasets are fused (10). Therefore, by fusing multiple real-time 3DE recordings taken from multiple acoustic windows (such as parasternal, standard apical, non-standard apical and subcostal windows) it is possible to generate a M3DFE dataset which is of superior quality to that ever previously achieved by conventional 3DE. Such a dataset could display the entire heart given the expected vast FOV. This would facilitate study of other cardiac structures such as the right ventricle, left atrium and cardiac valves.

In addition, future advances have the ability to enhance the clinical feasibility of M3DFE. For example, respiratory-gating techniques could allow acquisition of datasets during free-breathing, and similar respiratory tracking input as collected in this study could be used to correct for patient movement in the spatial alignment process such that patients do not have to remain still.

5. Conclusion

The real-time M3DFE technique evaluated in this study is the first to effectively screen for diagnostically suitable M3DFE datasets by quantitatively assessing mean chest marker displacement. The success of this protocol represents a significant step forward in the feasibility and effectiveness of M3DFE, a modality which we now believe is ready for clinical trials. Both fusion by voxel averaging and wavelet decomposition are effective methods of M3DFE which result in increased ΔFOV and both subjective and objective improvements in image quality. Results suggest wavelet decomposition is a superior fusion technique to voxel averaging. While the results of this study on healthy volunteers are promising, further works validating M3DFE in a clinical setting are required before this modality is ready for mainstream clinical use.

6. Chapter 2 Tables and Figures

	Number of Segments	Contrast (mean ± SD)	CNR (mean ± SD)	SNR (mean ± SD)	EBD (mean ± SD)
Unmoving Transducer: SSA	101	74.1 ± 14.5	11.8 ± 5.0	17.9 ± 4.6	0.89 ± 0.22
Unmoving Transducer: M3DFE AVG	101	73.5 ± 11.0	18.5 ± 5.8	29.6 ± 7.6	1.10 ± 0.33
Unmoving Transducer: M3DFE WAV	101	77.1 ± 12.3	19.9 ± 6.8	32.7 ± 7.6	1.22 ± 0.32
Moving Transducer: NSA - SSA	111	77.6 ± 18.1	14.6 ± 6.1	19.1 ± 4.9	1.06 ± 0.23
Moving Transducer: NSA - M3DFE AVG	111	70.3 ± 14.3	24.1 ± 7.8	33.4 ± 7.2	1.20 ± 0.36
Moving Transducer: NSA - M3DFE WAV	111	77.0 ± 17.8	22.3 ± 11.6	33.2 ± 15.1	1.36 ± 0.4
Moving Transducer: AP - SSA	77	88.9 ± 20.2	18.6 ± 8.7	22.1 ± 7.8	1.29 ± 0.20
Moving Transducer: AP - M3DFE AVG	77	67.7 ± 13.0	32.7 ± 6.7	28.3 ± 7.8	1.34 ± 0.26
Moving Transducer: AP - M3DFE WAV	77	88.8 ± 17.8	25.8 ± 11.5	35.6 ± 14.1	1.75 ± 0.24

Chapter 2, Table 1: Number of segments analyzed and mean ± standard deviation for contrast, CNR, SNR and EBD for each group within the three imaging protocols at end-systole. M3DFE = Multi-view 3D Fusion Echocardiography, SSA = Single Standard Apical, AVG = fusion by voxel averaging, WAV = fusion by wavelet decomposition, NSA = non-standard apical group, AP-PS = apical-parasternal group, CNR = contrast-to-noise ratio, SNR = signal-to-noise ratio, EBD = endocardial border definition.

	Number of Segments	Contrast (mean ± SD)	CNR (mean ± SD)	SNR (mean ± SD)	EBD (mean ± SD)
Unmoving Transducer: SSA	96	79.6 ± 11.1	16.5 ± 7.8	22.2 ± 6.8	0.89 ± 0.24
Unmoving Transducer: M3DFE AVG	96	75.6 ± 11.9	23.3 ± 8.3	33.8 ± 8.0	1.13 ± 0.34
Unmoving Transducer: M3DFE WAV	96	78.9 ± 12.5	23.7 ± 7.7	36.0 ± 8.1	1.23 ± 0.28
Moving Transducer: NSA - SSA	100	87.8 ± 15.5	20.9 ± 29.3	24.2 ± 35.1	1.03 ± 0.35
Moving Transducer: NSA - M3DFE AVG	100	80.5 ± 14.9	29.3 ± 12.0	35.1 ± 10.4	1.22 ± 0.41
Moving Transducer: NSA - M3DFE WAV	100	86.6 ± 16.4	30.4 ± 14.3	38.6 ± 13.6	1.30 ± 0.38
Moving Transducer: AP - SSA	77	84.8 ± 16.3	18.6 ± 10.7	20.9 ± 10.8	1.31 ± 0.34
Moving Transducer: AP - M3DFE AVG	77	69.5 ± 9.1	25.0 ± 10.3	29.7 ± 9.7	1.38 ± 0.36
Moving Transducer: AP - M3DFE WAV	77	82.7 ± 16.5	26.6 ± 12.7	34.6 ± 13.8	1.71 ± 0.26

Chapter 2, Table 2: Number of segments analyzed and mean ± standard deviation for contrast, CNR, SNR and EBD for each group within the three imaging protocols at end-diastole. M3DFE = Multi-view 3D Fusion Echocardiography, SSA = Single Standard Apical, AVG = fusion by voxel averaging, WAV = fusion by wavelet decomposition, NSA = non-standard apical group, AP-PS = apical-parasternal group, CNR = contrast-to-noise ratio, SNR = signal-to-noise ratio, EBD = endocardial border definition.

	Contrast %Diff. in Means	**CNR** %Diff. in Means	**SNR** %Diff. in Means	**EBD** %Diff. in Means
Unmoving Transducer: **M3DFE (AVG) – SSA**	-0.9% p = 0.55	+57% p < 0.0001	+65% p = 0.00001	+24% p = 0.0004
Unmoving Transducer: **M3DFE (WAV) – SSA**	+4.1% p = 0.06	+44% p < 0.00001	+50% p < 0. 000001	+30% p < 0.00001
Unmoving Transducer: **M3DFE (WAV) – M3DFE (AVG)**	+4.9% p = 0.02	+12% p = 0.25	+18% p = 0.14	+14% p = 0.03
Moving Transducer: NSA **M3DFE (AVG) – SSA**	-9.4% p = 0.43	+65% p = 0.01	+75% p = 0.005	13% p = 0.054
Moving Transducer: NSA **M3DFE (WAV) – SSA**	+0.9% p = 0.49	+32% p = 0.03	+42% p = 0.006	25% p = 0.0002
Moving Transducer: NSA **M3DFE (WAV) – M3DFE (AVG)**	+8.6% p = 0.10	-12% p = 0.43	-1.4% p = 0.50	+16% p = 0.02
Moving Transducer: AP **M3DFE (AVG) – SSA**	-24% p = 0.99	+17% p = 0.27	+28% p = 0.12	+4% p = 0.39
Moving Transducer: AP **M3DFE (WAV) – SSA**	+0.6% p = 0.50	+41% p = 0.009	+55% p < 0.001	+35% p = 0.00001
Moving Transducer: AP **M3DFE (WAV) – M3DFE (AVG)**	+24% p = 0.0001	+31% p = 0.07	+42% p = 0.03	+32% p < 0.0001

Chapter 2, Table 3: Results of one-tailed ANOVA test with Tukey Honest Significant Difference post-hoc correction at end-systole. Statistically significant results which reject the null hypothesis are highlighted in green. M3DFE = Multi-view 3D Fusion Echocardiography, SSA = Single Standard Apical 3DE, AVG = fusion by voxel averaging, WAV = fusion by wavelet decomposition, NSA = non-standard apical protocol, AP = apical-parasternal protocol, CNR = contrast-to-noise ratio, SNR = signal-to-noise ratio, EBD = endocardial border definition.

	Contrast %Diff. in Means	**CNR** %Diff. in Means	**SNR** %Diff. in Means	**EBD** %Diff. in Means
Unmoving Transducer: **M3DFE (AVG) – SSA**	-4.9% p = 0.98	+42% p = 0.008	+52% p < 0.001	+27% p < 0.0001
Unmoving Transducer: **M3DFE (WAV) – SSA**	-0.8% p = 0.45	+31% p = 0.005	+41% p = 0.0001	+30% p < 0. 000001
Unmoving Transducer: **M3DFE (WAV) – M3DFE (AVG)**	+4.1% p = 0.046	+2.5% p = 0.49	+9.8% p = 0.36	+10% p = 0.07
Moving Transducer: NSA **M3DFE (AVG) – SSA**	-8.2% p = 0.99	+40% p = 0.00072	+45% p < 0.001	+18% p = 0.002
Moving Transducer: NSA **M3DFE (WAV) – SSA**	-1.4% p = 0.45	+32% p = 0.0002	+41% p < 0.0001	+22% p < 0.0001
Moving Transducer: NSA **M3DFE (WAV) – M3DFE (AVG)**	+6.9% p = 0.03	+5.0% p = 0.43	+14% p = 0.20	+8.1% p = 0.12
Moving Transducer: AP **M3DFE (AVG) – SSA**	-18% p = 0.99	+34% p = 0.01	+42% p < 0.001	+4.8% p = 0.35
Moving Transducer: AP **M3DFE (WAV) – SSA**	-3.1% p = 0.38	+32% p = 0.003	+47% p < 0.00001	+29% p = 0.0001
Moving Transducer: AP **M3DFE (WAV) – M3DFE (AVG)**	+16% p < 0.001	+8.4% p = 0.38	+24% p = 0.04	+26% p < 0.001

Chapter 2, Table 4: Results of one-tailed ANOVA test with Tukey Honest Significant Difference post-hoc correction at end-diastole. Statistically significant results which reject the null hypothesis results are highlighted in green. M3DFE = Multi-view 3D Fusion Echocardiography, SSA = Single Standard Apical 3DE, AVG = fusion by voxel averaging, WAV = fusion by wavelet decomposition, NSA = non-standard apical protocol, AP-PS = apical-parasternal protocol, CNR = contrast-to-noise ratio, SNR = signal-to-noise ratio, EBD = endocardial border definition.

Variable	Type of Variable	Test	Result	Interpretation
Contrast	Continuous	ICC	0.65	**Good Agreement**
SNR	Continuous	ICC	0.27	**Poor Agreement**
CNR	Continuous	ICC	0.40	**Moderate Agreement**
EBD	Categorical	Weighted Kappa	0.51	**Moderate Agreement**

Chapter2, Table 5: Inter-rater Agreement Analysis. ICC = Intra-class correlation coefficient. SNR = Signal-to-noise ratio. CNR = Contrast-to-noise ratio. EBD = Endocardial Border Definition.

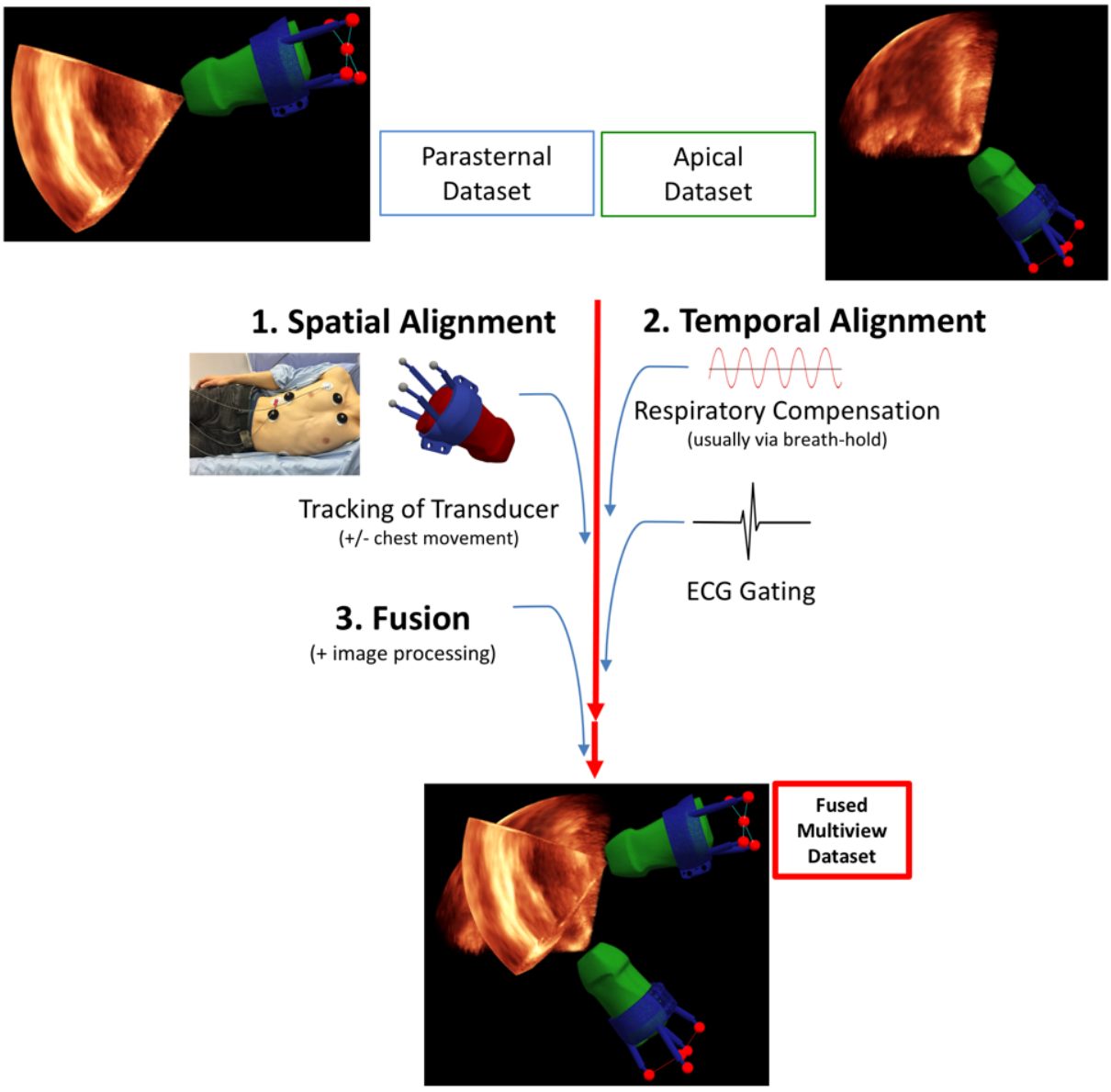

Chapter 2, Figure 1: Steps required to produce a M3DFE dataset.

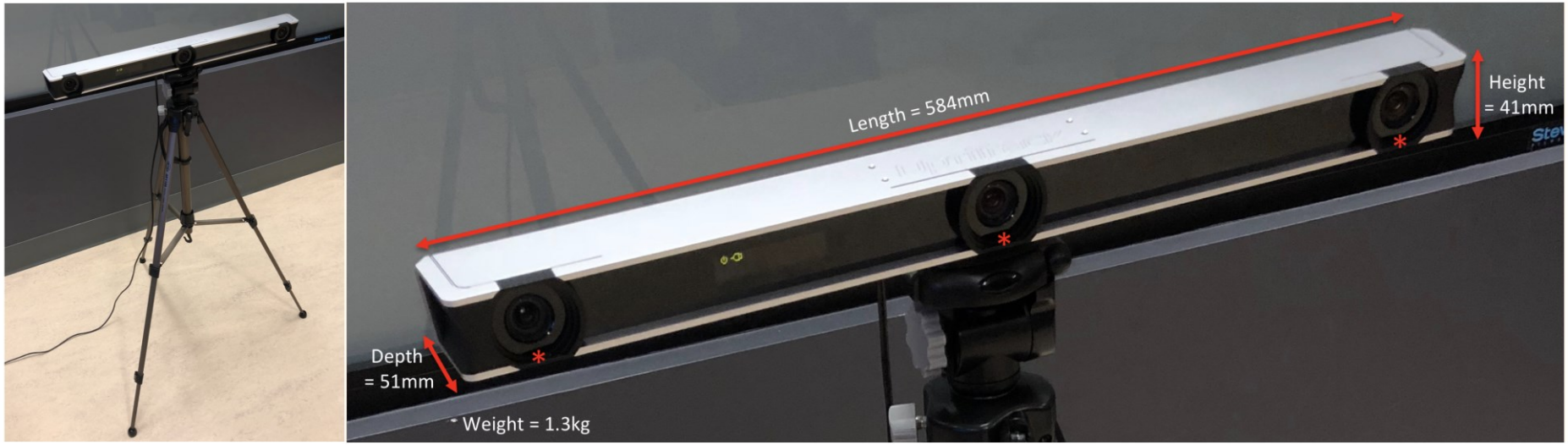

Chapter 2, Figure 2: The optical tracking device containing 3 infrared cameras (+tripod, left; zoomed view, right) used to track transducer and chest marker position in our study (OptiTrack V120:Trio, 6 degrees of freedom, resolution 640x480 x 3, refresh rate 120Hz). The height of the tripod ranged from approximately 120-150cm and was individualized to optimize the line of sight between the cameras and both the transducer and markers. Asterisks correspond to each of the three infrared cameras.

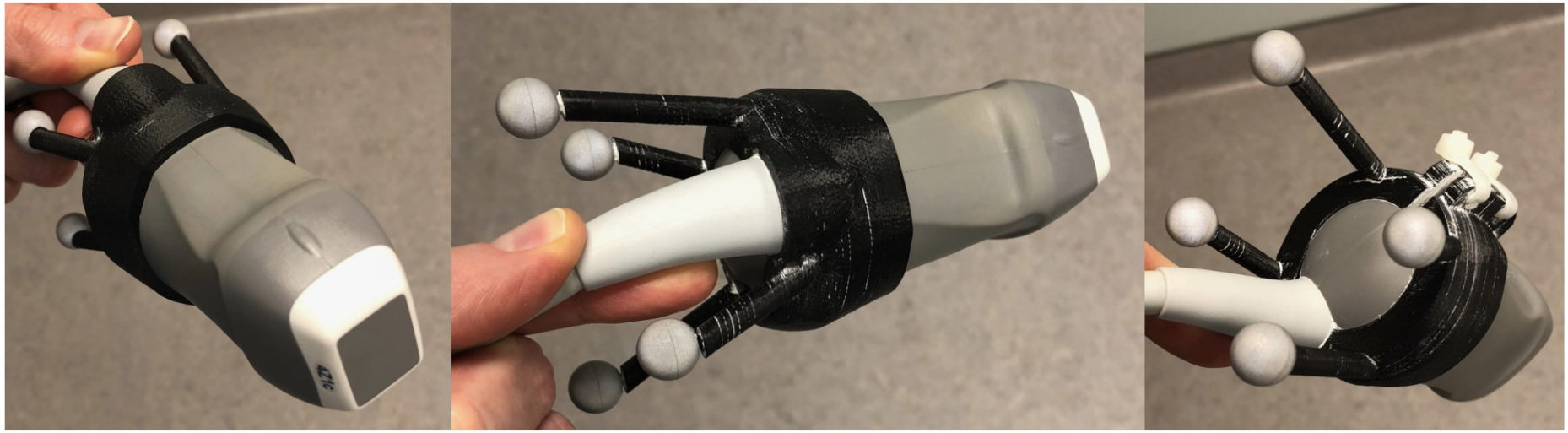

Chapter 2, Figure 3: Siemens 4Z1c matrix array transducer with mount/marker apparatus. Note the four silver spherical infrared markers attached to the mount (black). The 3D position and orientation of the markers (and by extension, the transducer) were tracked by the cameras through their preferential reflection of infrared light. The black mount was created using a 3D printer and consists of a plant-based, biodegradable and recyclable compound which is a blend of polylactic acid and polyhydroxyalkanoate (material by ColorFabb®).

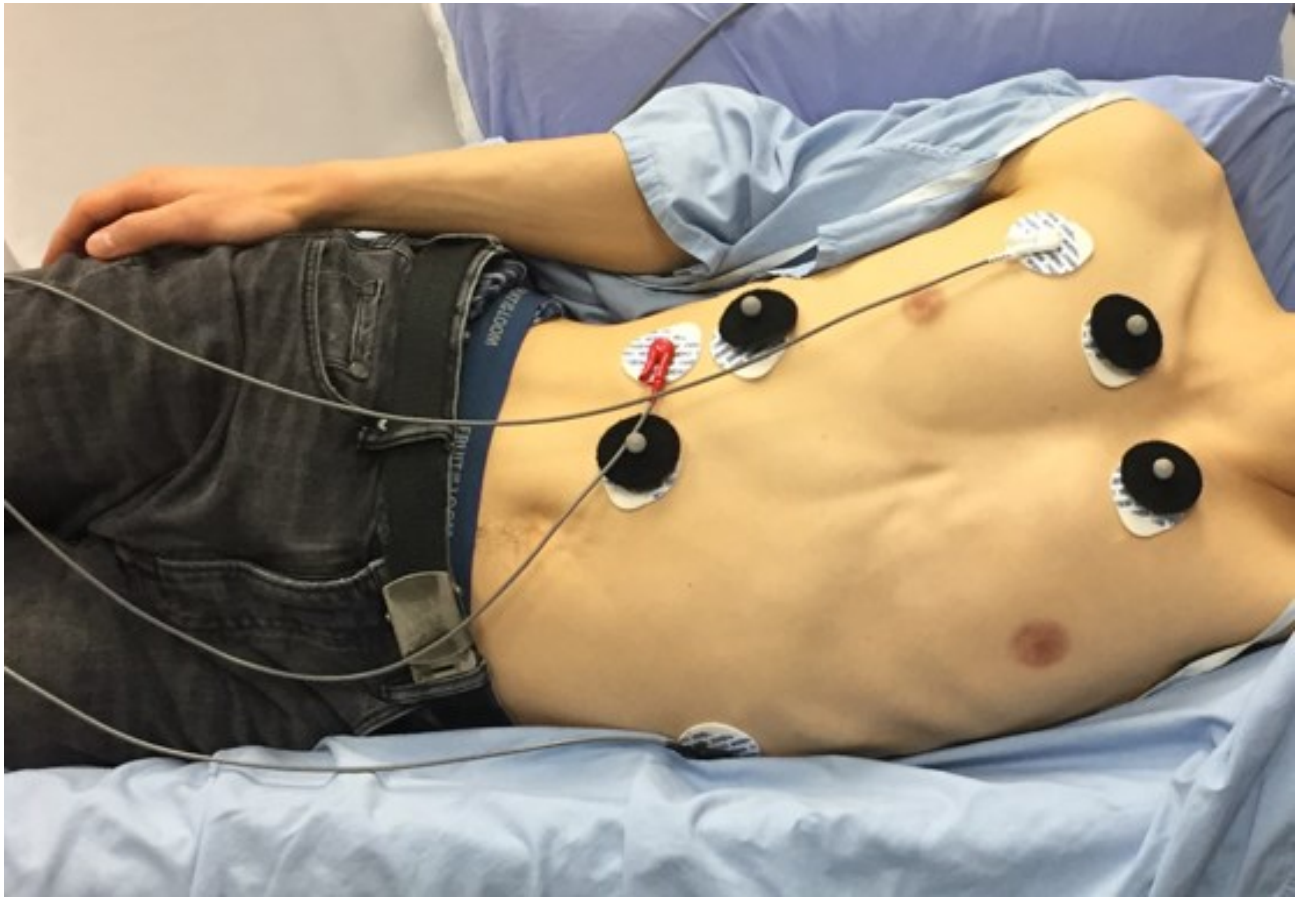

Chapter 2, Figure 4: Chest markers affixed to the ECG stickers. These markers preferentially reflect infrared light in the same way the transducer markers do, allowing real-time monitoring of patient breathing and movement during echocardiographic recordings.

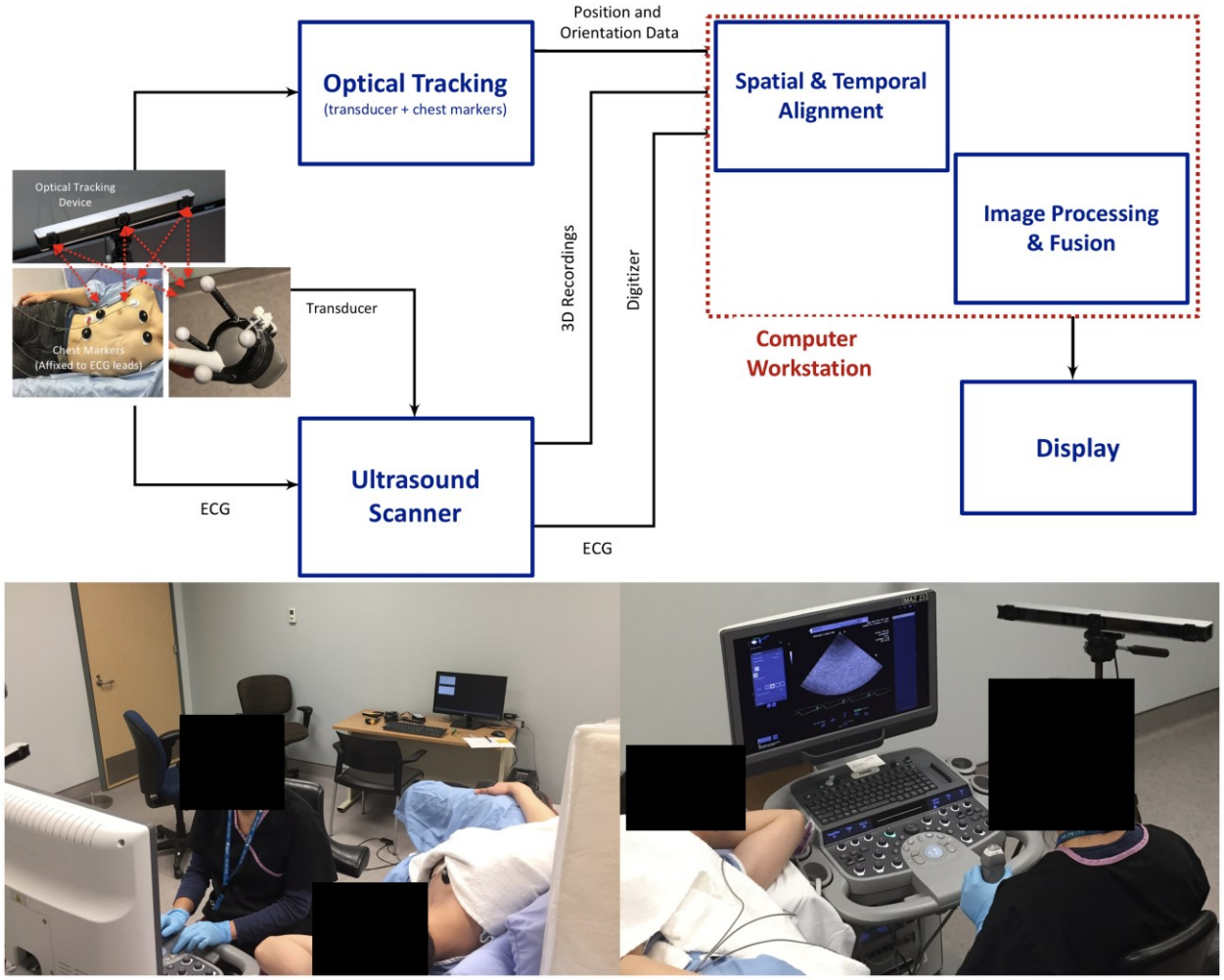

Chapter 2, Figure 5: M3DFE components and setup. A schematic diagram demonstrating the relationship between each of the necessary components (top center). The relative positions of the infrared cameras, ultrasound scanner, sonographer and study subject are shown (left). The computer used for 3D tracking and data collection is also shown (right).

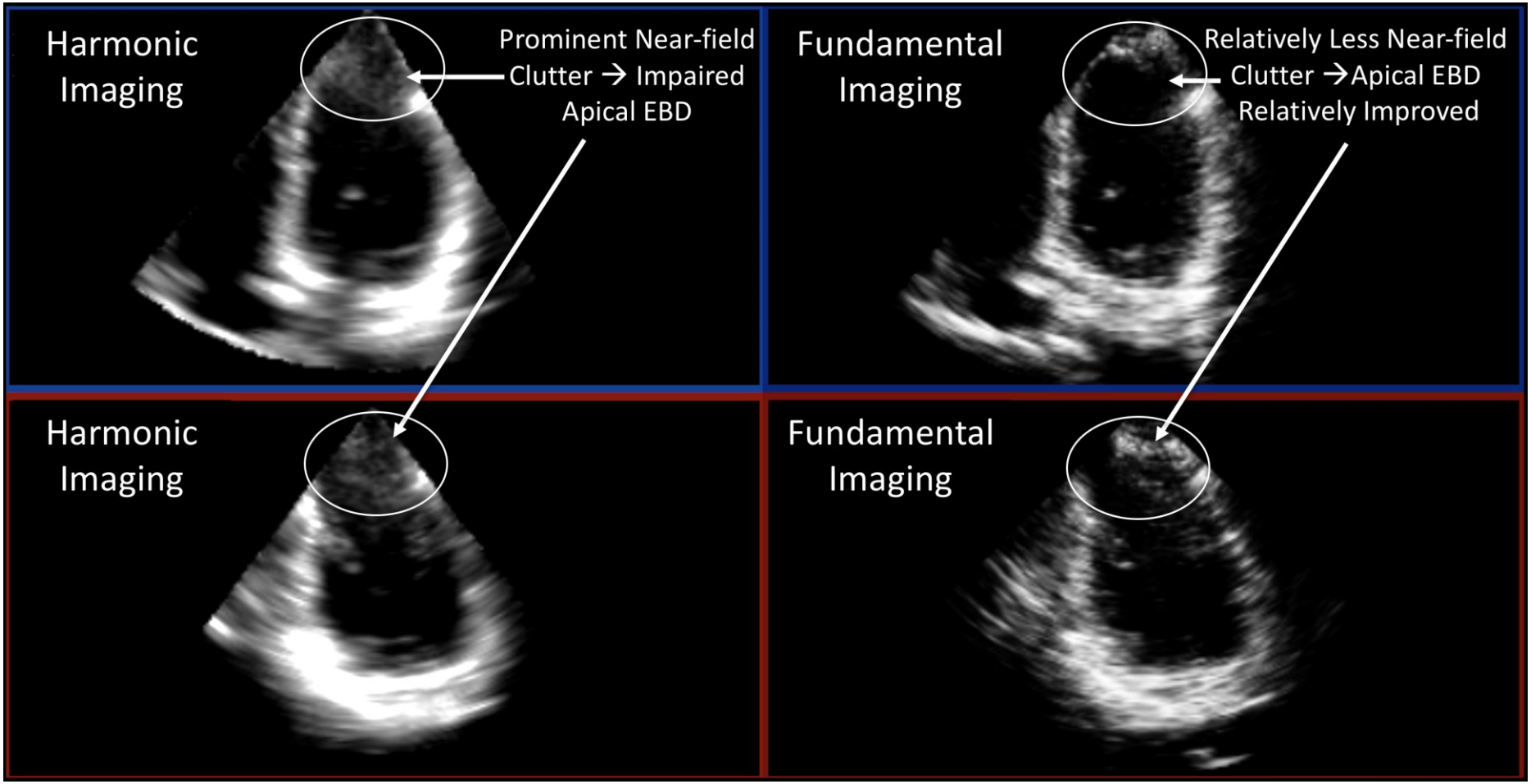

Chapter 2, Figure 6: Fundamental frequency imaging was used for apical windows as near-field clutter artifacts seen with harmonic imaging (left) were much less prominent when imaging with fundamental frequencies (right).

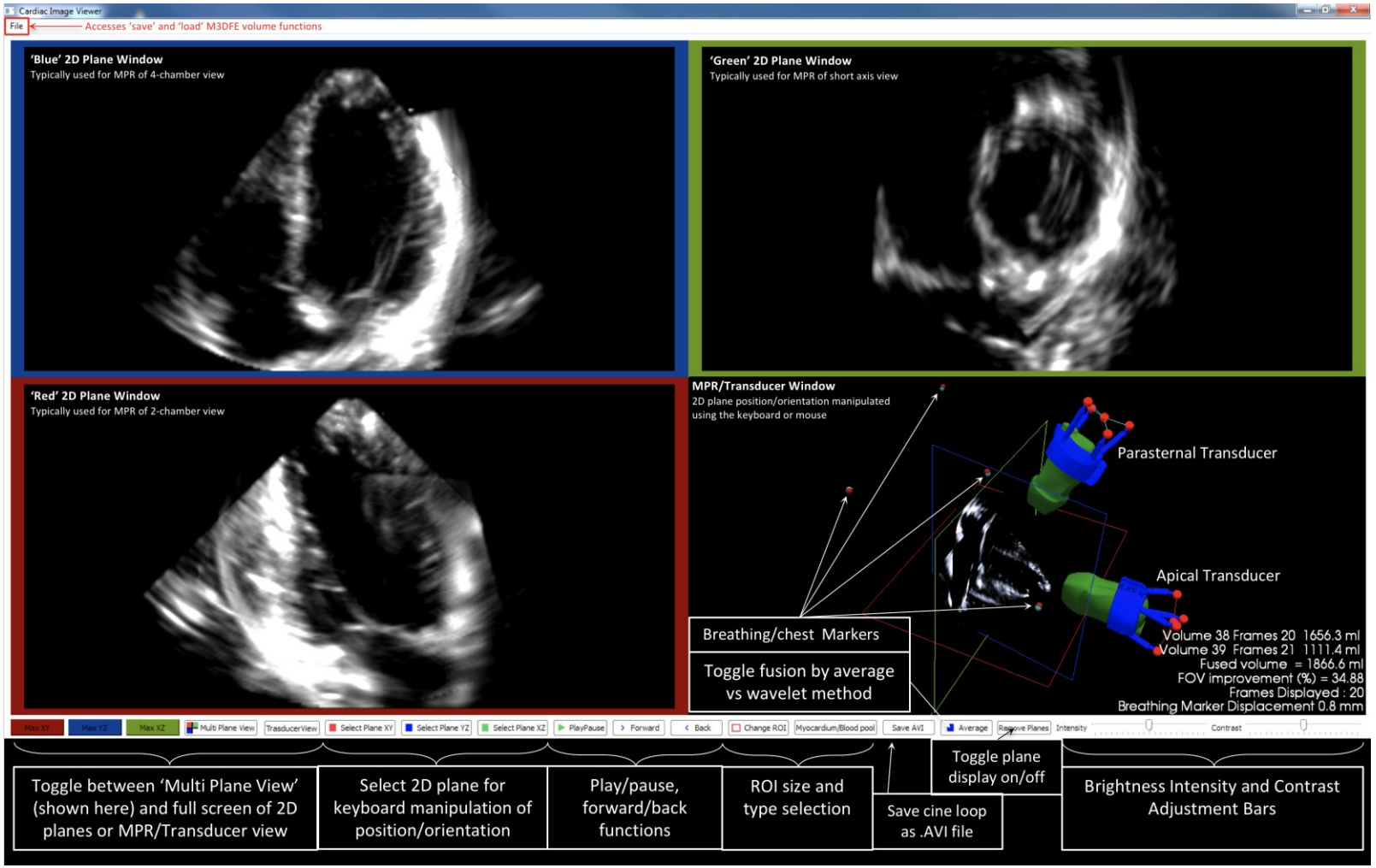

Chapter 2, Figure 7: Screenshot of the M3DFE software viewer custom built for this project. A M3DFE volume comprised of one apical and one parasternal volume fused using the wavelet method is shown. Descriptions are seen in white text. MPR = Multi-planar reconstruction, ROI = Region of interest, 2D = 2-dimensional, FOV = field of view.

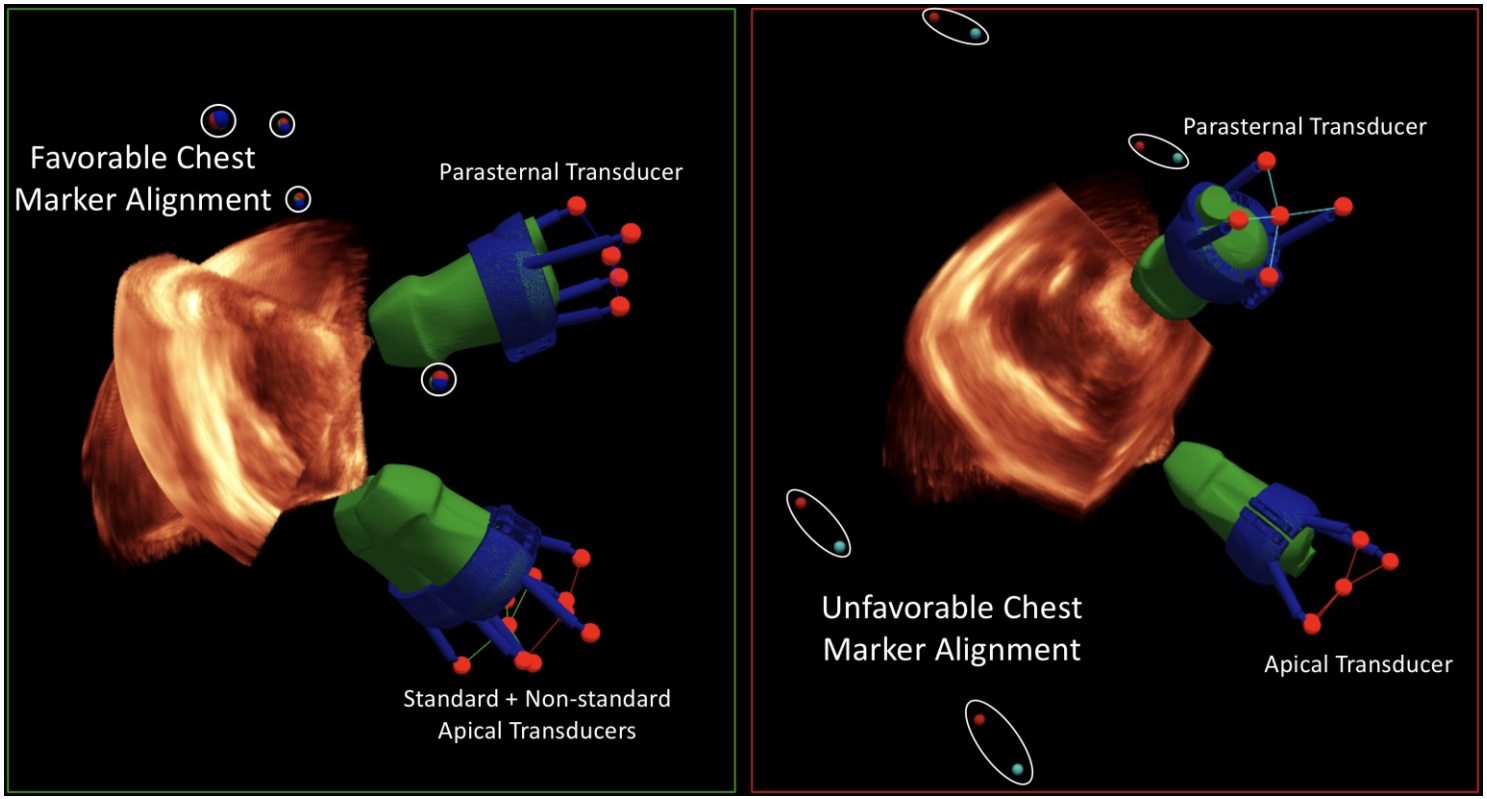

Chapter 2, Figure 8: 3D rendering of two M3DFE datasets illustrating favorable vs. unfavorable chest marker alignment. Left: An ideal M3DFE recording shows chest markers essentially superimposed on one another as demonstrated by the small white circles encompassing each set of markers. The mean chest marker displacement was 0.2mm in this case. This finding confirms the subject remained still and maintained an effective breath-hold maneuver and is predictive of successful spatial alignment. Right: A suboptimal M3DFE recording shows markers which are widely separated as demonstrated by the larger ellipses encompassing each set of markers. The mean chest marker distance was 4.5mm in this case, which is much greater than the 1.5mm threshold resulting in exclusion in this study, and is predictive of poor spatial alignment.

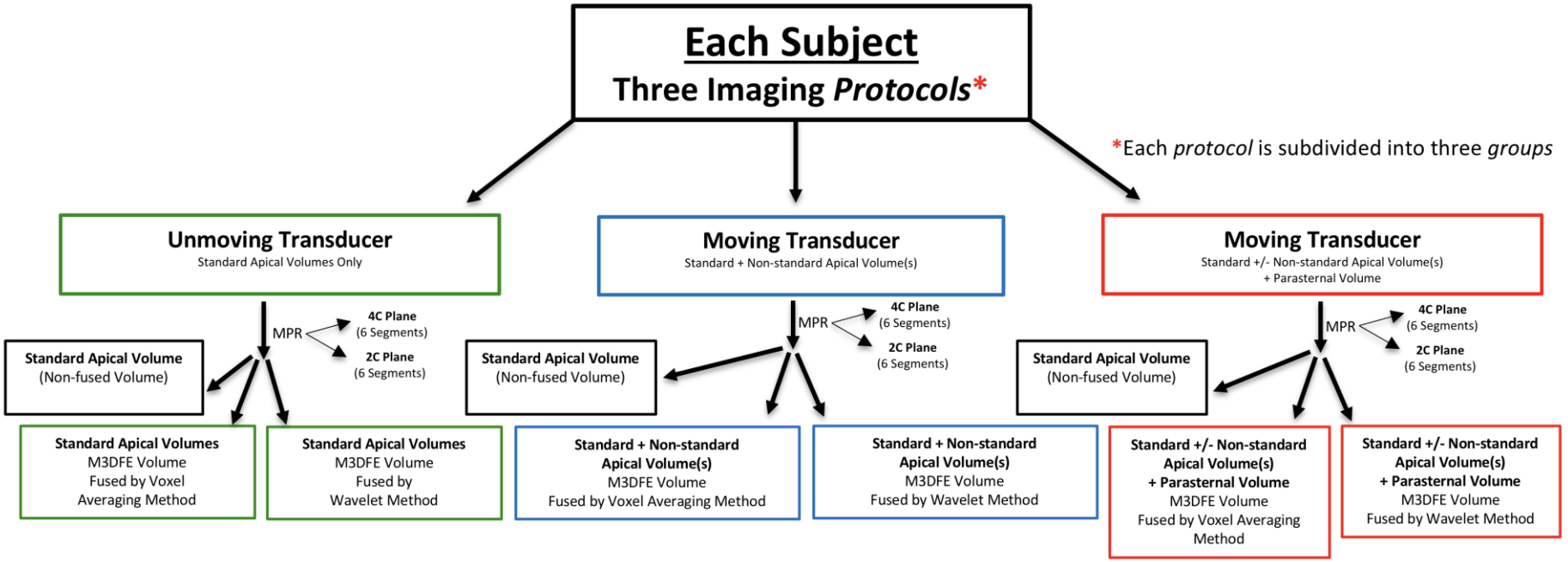

Chapter 2, Figure 9: Study design. This protocol was performed x 2 (end-systole + end-diastole). MPR = Multi-planar Reconstruction of 3DE volume. 2C = 2-chamber. 4C = 4-chamber.

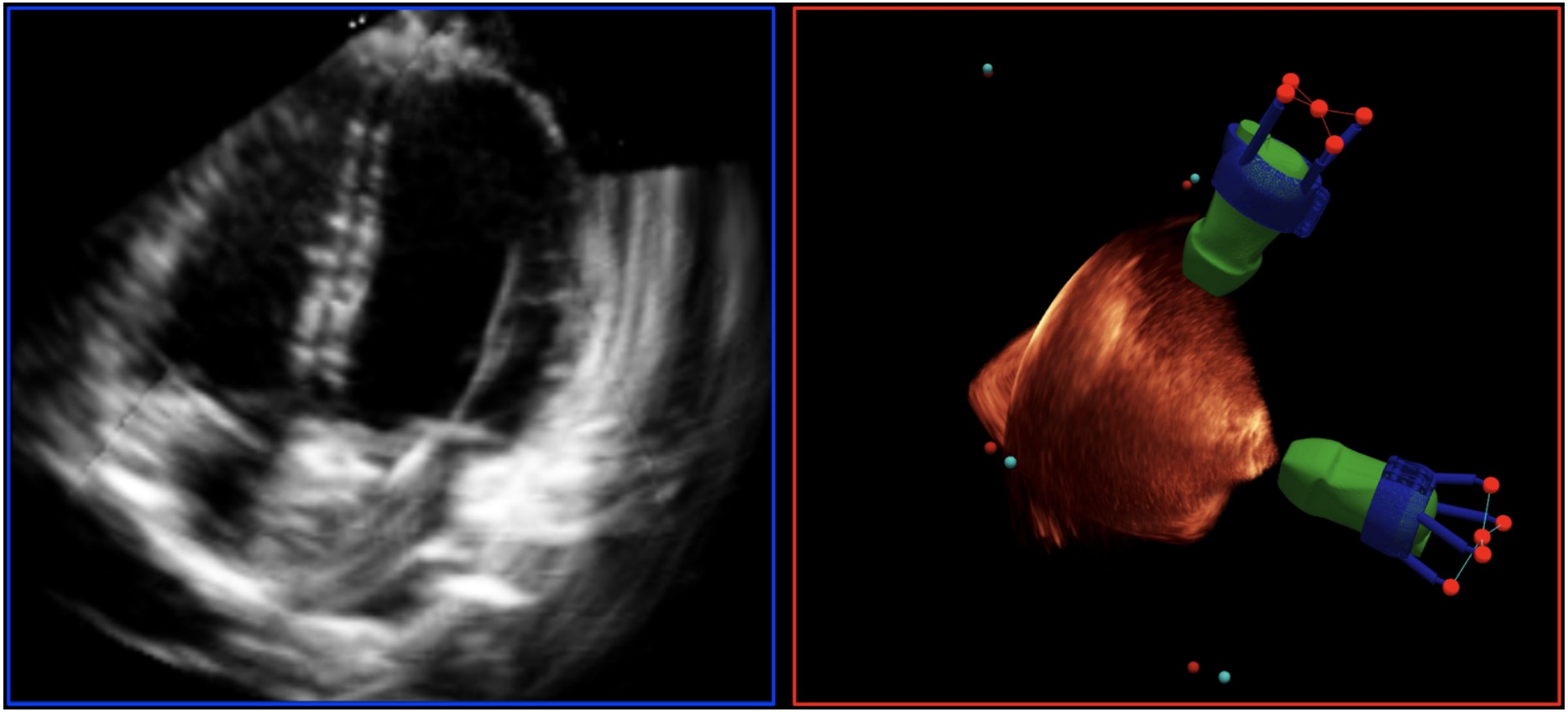

Chapter 2, Figure 10: A M3DFE volume demonstrating poor alignment (left). Note the double-contoured interventricular septum. In this case, the mean chest marker displacement was 3.2mm – far greater than the threshold for exclusion of 1.5mm. The corresponding transducer/marker display is shown (right).

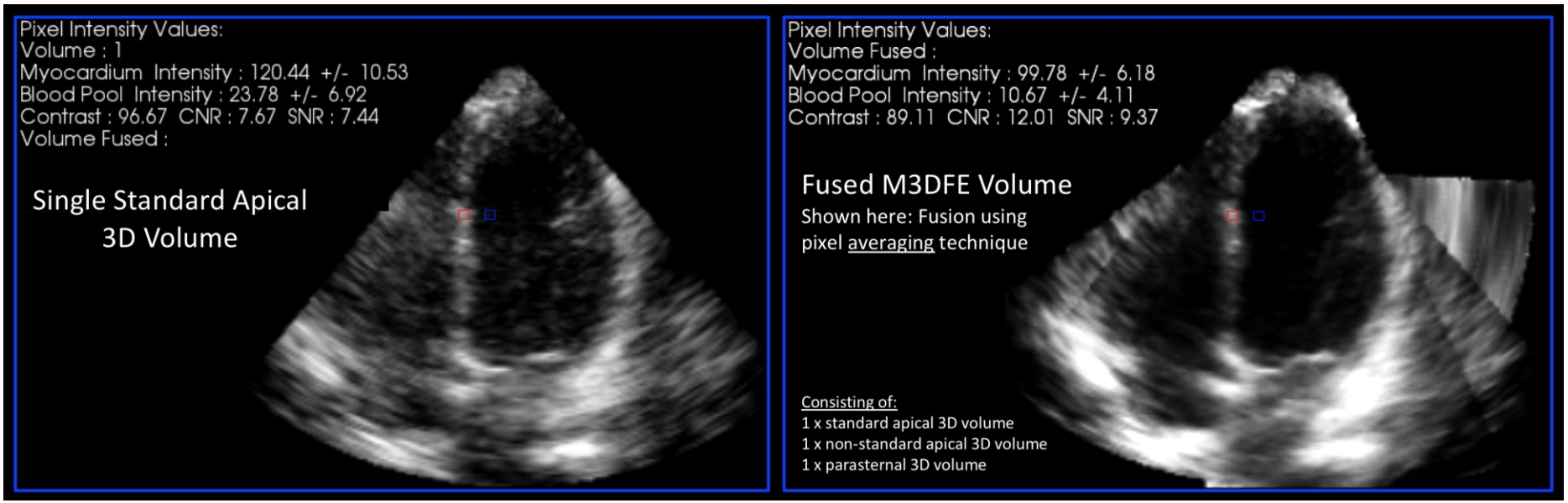

Chapter 2, Figure 11: Derivation of contrast, CNR and SNR values as shown here using an example multi-planar reconstructed 4-chamber view. Region of interest boxes were placed in the myocardium (red) and adjacent LV cavity (blue). Mean and standard deviations of pixel intensity within the regions of interest were used to automatically generate contrast, CNR and SNR values for each of the 6 standard myocardial segments in both the 4- and 2-chamber views.

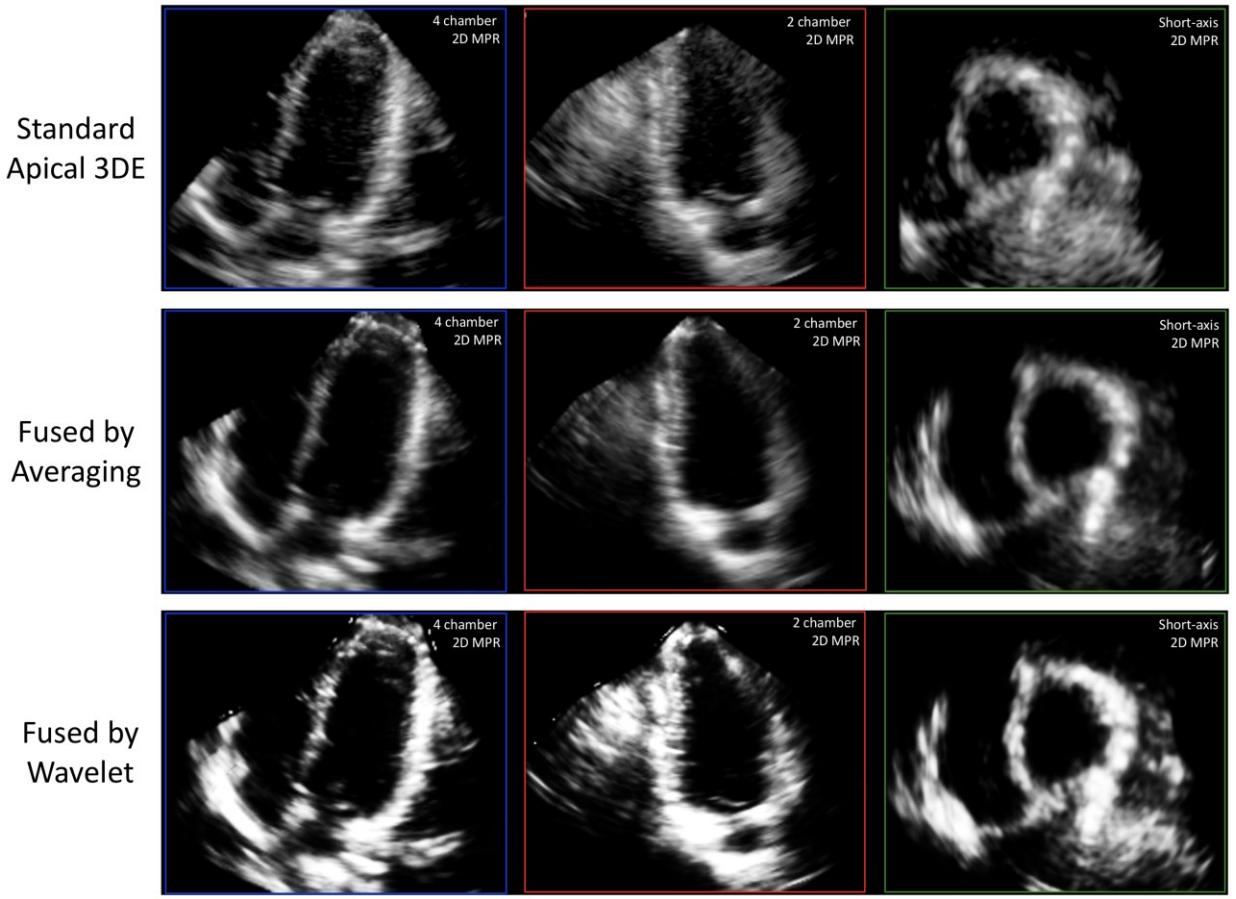

Chapter 2, Figure 12: An example comparison of a non-fused single standard apical 3DE volume (top row), fused M3DFE consisting of the same standard apical 3DE volume as in the top row plus two additional non-standard apical 3DE volumes fused by the voxel averaging method (middle row) and fused using the wavelet method (bottom row). Note the enhanced myocardial signal / endocardial border definition, reduction in LV cavity noise, greatly improved visualization of the anterior wall (best seen in the 2-chamber view), and the increased FOV to display more of the right ventricle (best seen in the short-axis view). MPR = multi-planar reconstruction.

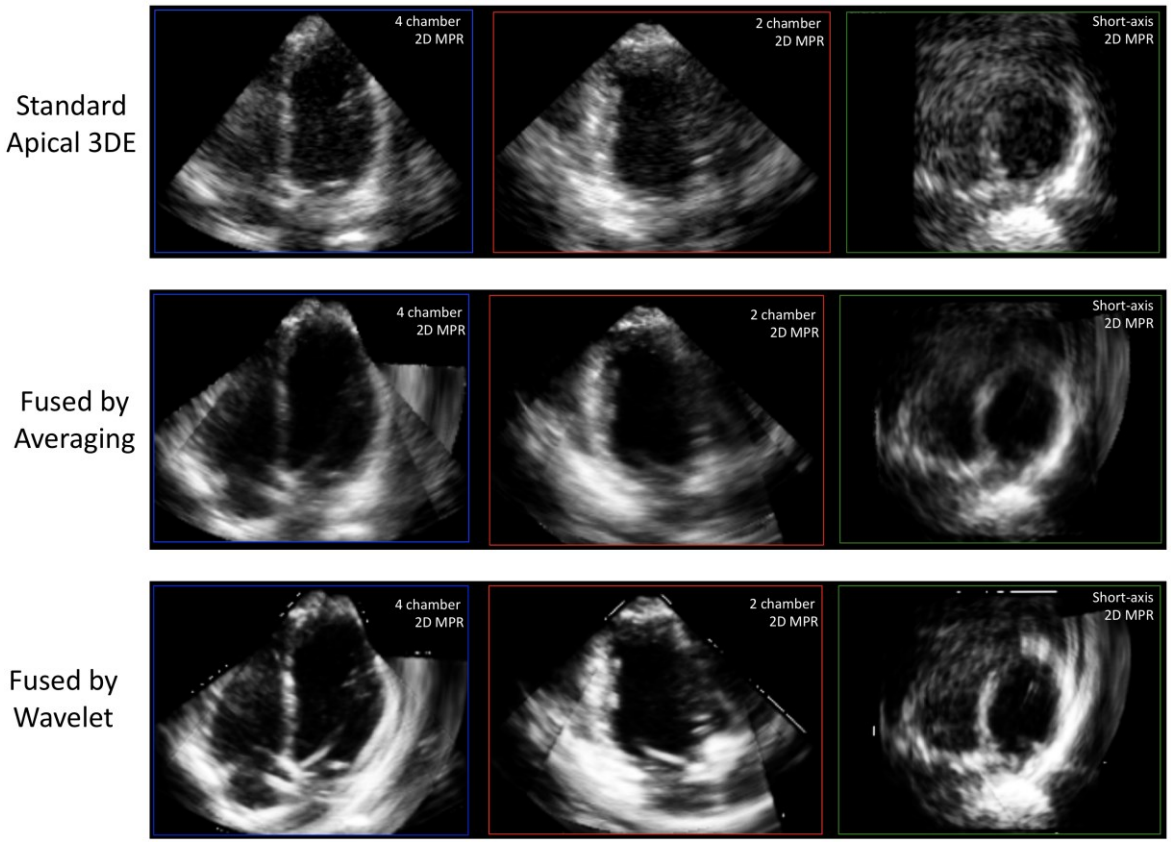

Chapter 2, Figure 13: An example comparison of a non-fused single standard apical 3DE volume (top row), fused M3DFE consisting of the same standard apical 3DE volume as in the top row plus both a non-standard apical volume 3DE and a parasternal 3DE volume fused by the voxel averaging method (middle row) and fused using the wavelet method (bottom row). Note the enhanced visibility of the RV and LV apex as well as the reduced noise seen with both fusion methods. Also note the diluted myocardial signal in the region of overlap that is characteristic of the fusion by averaging method (especially prominent in the interventricular septum). This is recovered when applying the fusion by wavelet decomposition method.

Chapter III

Future Directions and Conclusions

1. Future Directions

1.1 Maximizing the Potential of Ultrasound with Multi-view 3D Fusion Echocardiography

There are additional ways in which multi-view 3D fusion echocardiography (M3DFE) could be used to maximize the potential of ultrasound to enhance image quality. Using what we know of ultrasound physics, it is possible to optimize image quality in regions of interest by choosing appropriate equipment and by manipulating machine settings. If one performs such assessments on various regions of interest, then fuses the resulting 3DE (3-dimensional echocardiography) recordings, the expected result is a synergistic dataset of superior overall quality. We applied this strategy in Chapter II, where fundamental imaging was used from the apical window to optimize the near-field (apex of the left ventricle (LV)), while harmonic imaging was used from the parasternal window to optimize the mid- and far-fields (mid and basal LV).

Another approach to optimizing the spatial and temporal resolution of the LV apex could involve using a high-frequency transducer (or high-frequency 'resolution' setting) while imaging at a reduced depth with a shallow focus and narrow sector angle. To optimize the spatial and temporal resolution of the mid/basal LV or atria (far-field) from an apical window, one might use a lower-frequency probe (or low-frequency 'penetration' setting) and a deep focal zone to maximize visibility of these structures. If one were to then fuse the resulting 3DE recordings, the expected result would be a M3DFE dataset with optimized image quality in both the near and far-fields.

One study assessing real-time M3DFE showed that greater benefits are achieved as progressively more 3DE volumes are fused (1). Therefore, if protocols were developed whereby multiple real-time 3DE recordings were taken from multiple acoustic windows, the overall benefits of M3DFE may be even greater than have been demonstrated thus far.

1.2 Respiratory Gating and 'Free-breathing Acquisitions'

Creation of M3DFE has, to date, required subjects to perform breath-holds during 3DE recordings. These tasks are usually not difficult for the young, healthy volunteers participating in most pre-clinical M3DFE studies but can be significantly challenging in older, unhealthy populations. It follows that, in order for M3DFE to establish itself as a mainstream imaging modality, it must evolve to remain feasible and effective when applied to a typical population seen in clinical practice. Some individuals in such a population are not able to perform the breath-holds currently required to create diagnostic M3DFE datasets. M3DFE must, therefore, ultimately evolve to allow its use during free-breathing.

One potential approach to conducting M3DFE during free-breathing begins with the acquisition of real-time 3DE recordings consisting of multiple successive beats. During 3DE recording, the amplitude of respiration is also monitored. Then, when performing temporal alignment, only those cardiac cycles occurring at specific times within the respiratory cycle are considered eligible for fusion (2). Since cardiac excursion is minimal during end-inspiration or end-expiration, 3DE recordings acquired near these phases of the respiratory cycle represent ideal candidates for fusion (Figure 1) (3). This process of data acquisition, which allows optimal temporal alignment via accounting for the respiratory cycle is referred to as 'respiratory gating'.

Various methods across many imaging modalities have been used to monitor the amplitude of the respiratory cycle in attempt to compensate for its effect. These methods could be considered for use in a respiratory gating procedure for M3DFE. Some methods directly monitor airflow through the nose or mouth using a spirometer or bellows (4). Others rely on the principle that abdominal contents are incompressible, and that inspiration should therefore result in abdominal protrusion and a corresponding increase in abdominal circumference (5). Two respiratory monitoring strategies based on measuring abdominal circumference include i) the use of devices, such as belts containing displacement transducers, which measure changes in abdominal circumference throughout respiration, and ii) optical tracking systems which can monitor the amplitude of respiration by tracking the movement of an optical marker attached to the umbilicus (shown to be the site of greatest abdominal excursion in at least one study)(6-8). ECG-electrodes can also be used to monitor the respiratory cycle by sensing changes in transthoracic impedance. This method is commonly used by ultrasound systems in the echocardiography laboratory to measure respirophasic

changes in cardiac physiology (9). These are just a few examples and do not represent an exhaustive list. Despite the many feasible options for respiratory monitoring, the method that would be best-suited for M3DFE is unknown and warrants further study.

1.3 Compensating for Patient Movement

Thus far, M3DFE datasets have been acquired with subjects remaining still to avoid problems of misaligned datasets resulting from changing body positions. However, remaining still for the duration of a M3DFE recording may not be feasible for all patients. It is therefore necessary that M3DFE evolve to allow at least minor degrees of patient movement. By tracking chest wall and transducer movement independently and simultaneously in a similar fashion to as performed in Chapter II, the dynamic spatial relationship between the two could be monitored, and corrected for, when creating a fused 3D dataset. Both optical and electromagnetic systems could be tested for this purpose. This is a proposed area of future study in our research laboratory. Ultimately, if such a technology could be implemented successfully alongside respiratory gating to allow for free-breathing, M3DFE would become a highly feasible modality in typical clinical settings.

1.4 Advancements in Electromagnetic Tracking

A major strength of electromagnetic (EM) tracking is that it is independent of the requirement for maintaining a line-of-sight between a camera and the transducer. However, EM tracking is currently limited by reduced accuracy compared to optical tracking, and most systems still require that the transducer is connected to an external computer via wires. However, advancements in electromagnetic (EM) tracking which are currently under study, such as improved accuracy and wireless sensors, have the potential to improve the feasibility of M3DFE in typical clinical laboratories (10).

1.5 Passive Robotic 'Measurement Arms' for Spatial Tracking

Tracking using a *passive robotic measurement arm* can be performed by affixing a robotic arm directly to an ultrasound transducer, and this approach has demonstrated feasibility in

pre-clinical phantom and animal tissue models (11, 12). The robotic arm is connected to a computer that directly records the 3D position of the transducer with remarkable accuracy – one recent paper quoted a translational accuracy of ~0.1mm and rotational error of ~ 0.03 degrees (11).

The sonographer performs the scan according to their usual protocol – the robotic arm does not independently move, but rather passively follows the transducer's movement and records its' position and orientation throughout the scan. The advantage of this method is avoidance of the line-of-site and bulky marker limitations of optical tracking while maintaining a high degree of accuracy. The disadvantage is that previously tested robotic arms have been too heavy and awkward for sonographers to manage beyond a few minutes, thereby limiting the feasibility of this approach (13). However, newer robotic arms that are lightweight and easier to maneuver are currently under investigation (13).

1.6 Enhancing Access to 3D Echocardiography

It is well known that cardiac sonography is technically challenging and requires highly trained and skilled personnel. Such personnel may not be accessible in certain settings, such as at small clinics or in remote communities (13). However, this limitation, which creates a barrier to delivery of echocardiography services in some cases, may be at least partially overcome by M3DFE. In such cases, M3DFE datasets can be generated using simple protocols whereby multiple recordings are obtained from closely located transducer positions. Such protocols would not necessarily require the same degree of skill as is typically provided by specialist sonographers. For example, a simple apical imaging protocol could be developed whereby a relatively unskilled technician creates a M3DFE dataset for purposes of LV volumetric analysis. Here, multiple acquisitions could be systematically recorded from i) a standard apical position plus ii) a set number of specific non-standard apical positions. Simple exclusion criteria could be applied to remove recordings containing significant artifacts. The resulting M3DFE dataset, generated by an unskilled individual, has the potential to match or even outperform the quality of a single 3DE recoding obtained by a skilled sonographer (14). The validity of this hypothesis obviously requires further study. However, if this theory proved true, it could have implications for laboratories suffering from sonographer shortages due to challenges with recruiting or due to budgetary constraints.

1.7 Going Beyond Transthoracic M3DFE and the Left Ventricle

While M3DFE has primarily been studied in the setting of *transthoracic* echocardiography, *transesophageal* echocardiography (TEE)-based M3DFE techniques have been recently investigated. This variation on M3DFE fuses 3DE recordings from multiple TEE views to create a single 3DE recording capable of visualizing all important anatomical landmarks in the left atrium (LA) (15). One such technique spatially aligns datasets using atlas-based mosaicking as an image registration tool and was demonstrated to be feasible in 16 cardiac surgical patients in the Netherlands (15).

The feasibility of another TEE-based fusion approach was demonstrated by Ren et al (16). Given the increasing performance of ablation procedures used to treat atrial fibrillation, a feasible and accurate TEE method which could accomplish the same goals as cardiac computed tomography (CCT) or cardiac magnetic resonance imaging (CMRI), while avoiding the associated radiation exposure and cost, would provide a very attractive alternative. Using this rationale, they performed a study aimed at developing a M3DFE protocol which can generate a map of the LA and pulmonary veins by extending the field-of-view (FOV) of 3D TEE and thus eliminate the need for pre-procedural CCT or CMRI.

M3DFE also holds promise for assessing structures beyond the left heart, and future protocols may provide a FOV so extensive that the entire heart can be reliably captured. This could allow a complete visualization of the geometrically complex right ventricle (RV). Multi-view fusion imaging has even been used to assess atheroma burden in studies using fusion to assess the carotid arteries and descending thoracic aorta. These non-cardiac applications of 3DE fusion provides proof that even fields such as vascular medicine may benefit from this technology in the future (17, 18).

2. Conclusions

M3DFE is an emerging 3DE modality with tremendous potential for advancing cardiac imaging. M3DFE has the ability to maximize the utility of diagnostic ultrasound by facilitating the 'fusion' of individual 3DE volumes containing redundant yet highly complementary information. This is achieved through the recording of multiple 3DE volumes using different

angles of insonation and/or various combinations of ultrasound equipment or machine settings. While M3DFE is technically challenging and complex, progressive advancements in spatial and temporal tracking, registration algorithms, software packages and imaging protocols promise to encourage its evolution in the ensuing years.

Given the growing body of literature supporting its use, and keeping in mind the promising findings delineated in Chapter II of this thesis, it is evident that M3DFE is ready for the next frontier of investigation – evaluating its feasibility and validity in the context of clinical trials.

3. Chapter 3 Figures

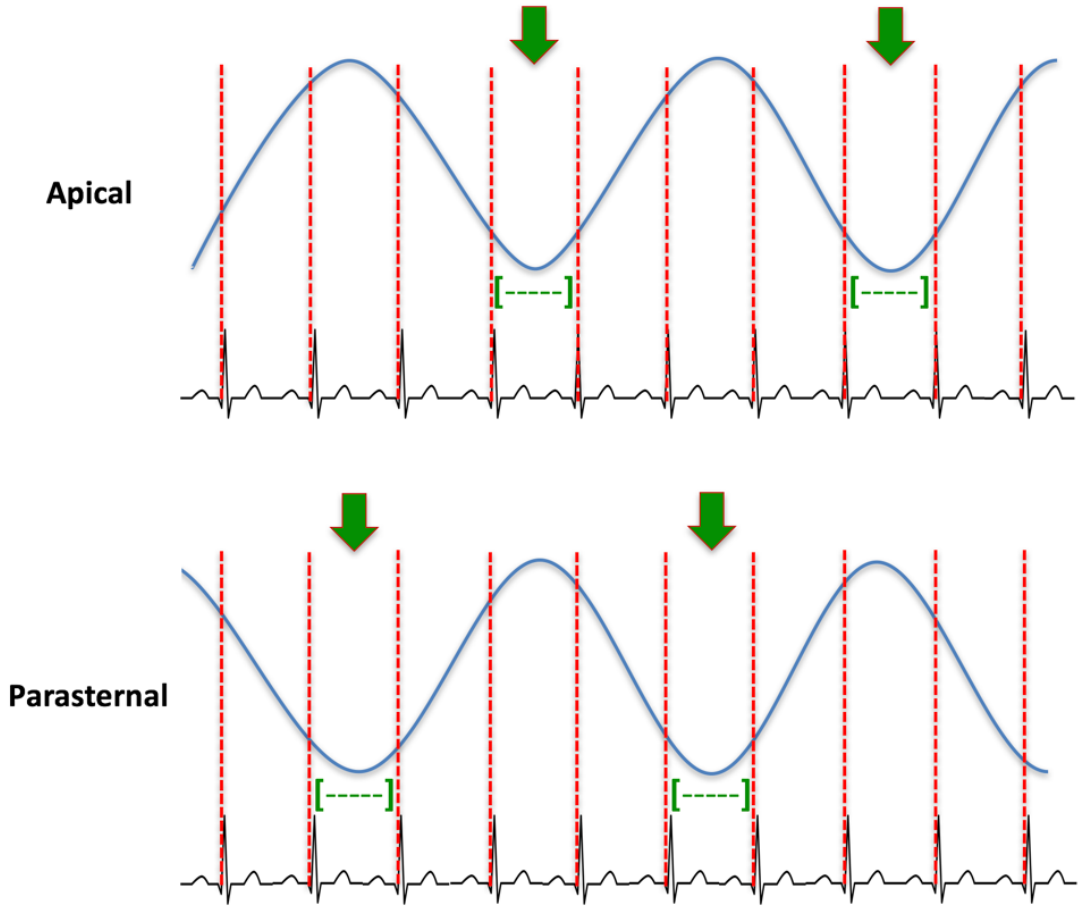

Chapter 3, Figure 1: Use of the ECG signal (black lines) and respiratory amplitude (blue lines) to perform respiratory gating on a multi-beat 3DE recording. Cardiac cycles are marked and the onset of the QRS complex (red dotted lines). Respiratory gating 'windows' are assigned to times within the respiratory cycle where cardiac/diaphragmatic excursion is minimal, such as around end-inspiration or end-expiration. In this case, gating windows are shown at end-expiration (green parentheses). Those cardiac cycles falling within the respiratory gating window are eligible for fusion – two such cardiac cycles recorded from each of the apical and parasternal windows would represent ideal intervals for 3DE recording and subsequent fusion (green arrows).

Bibliography

1. Chapter I:

1. Grau V, Becher H, Noble JA. Registration of multiview real-time 3-D echocardiographic sequences. IEEE Trans Med Imaging. 2007;26:1154-65.

2. Achenbach S, Friedrich MG, Nagel E*, et al*. CV imaging: what was new in 2012? J Am Coll Cardiol Img. 2013;6:714-34.

3. Lang RM, Bierig M, Devereux RB*, et al*. Recommendations for chamber quantification: a report from the American Society of Echocardiography's Guidelines and Standards Committee and the Chamber Quantification Writing Group, developed in conjunction with the European Association of Echocardiography, a branch of the European Society of Cardiology. J Am Soc Echocardiography. 2005;18:1440.

4. Perperidis A. Postprocessing Approaches for the Improvement of Cardiac Ultrasound B-Mode Images: A Review. IEEE Trans Ultrason Ferroelect Freq Control. 2016;63:470-85.

5. Lang RM, Badano LP, Mor-Avi V*, et al*. Recommendations for cardiac chamber quantification by echocardiography in adults: an update from the American Society of Echocardiography and the European Association of Cardiovascular Imaging. J Am Soc Echocardiogr. 2015;28:39.e14.

6. Danudibroto A, Bersvendsen J, Gerard O, Mirea O, D'hooge J, Samset E. Spatiotemporal registration of multiple three-dimensional echocardiographic recordings for enhanced field of view imaging. J Med Imaging. 2016;3:037001.

7. Rajpoot K, Grau V, Noble JA, Becher H, Szmigielski C. The evaluation of single-view and multi-view fusion 3D echocardiography using image-driven segmentation and tracking. Med Image Anal. 2011;15:514-28.

8. Lang RM, Badano LP, Tsang W*, et al*. EAE/ASE recommendations for image acquisition and display using three-dimensional echocardiography. J Am Soc Echocardiogr. 2012;13:1-46.

9. Grau V, Szmigielski C, Becher H, Noble JA. Combining apical and parasternal views to improve motion estimation in real-time 3D echocardiographic sequences. Proc IEEE Int Symp Biomed Imaging. 2008:516-9.

10. Tsang W, Salgo IS, Medvedofsky D*, et al*. Transthoracic 3D Echocardiographic Left Heart Chamber Quantification Using an Automated Adaptive Analytics Algorithm. J Am Coll Cardiol Img. 2016;9:769-82.

11. Leung KYE, van Stralen M, van Burken G, de Jong N, Bosch JG. Automatic active appearance model segmentation of 3D echocardiograms. Paper presented at: IEEE International Symposium on Biomedical Imaging: From Nano to Macro, 2010.
12. Noble JA, Navab N, Becher H. Ultrasonic image analysis and image-guided interventions. Interface Focus. 2011;1:673-85.
13. Wang F, Vemuri BC. Non-Rigid Multi-Modal Image Registration Using Cross-Cumulative Residual Entropy. Int J Comput Vis. 2007;74:201-15.
14. Sra J. Cardiac Image Registration. J Atr Fibrillation. 2008;1:24-41.
15. Venderink W, de Rooij M, Sedelaar JPM, Huisman HJ, Futterer JJ. Elastic Versus Rigid Image Registration in Magnetic Resonance Imaging-transrectal Ultrasound Fusion Prostate Biopsy: A Systematic Review and Meta-analysis. Eur Urol Focus. 2016.
16. Hipwell JH, Vavourakis V, Han L, Mertzanidou T, Eiben B, Hawkes DJ. A review of biomechanically informed breast image registration. Phys Med Biol. 2016;61:1.
17. Zhang W, Noble JA, Brady JM. Adaptive non-rigid registration of real time 3D ultrasound to cardiovascular MR images. Inf Process Med Imaging. 2007;20:50-61.
18. Wein W, Camus E, John M*, et al*. Towards guidance of electrophysiological procedures with real-time 3D intracardiac echocardiography fusion to C-arm CT. Med Image Comput Comput Assist Interv. 2009;12:9-16.
19. Rajpoot K, Grau V, Noble JA, Szmigielski C, Becher H. Multiview Fusion 3-d Echocardiography: Improving the Information and Quality of Real-Time 3-D Echocardiography. Ultrasound Med Biol. 2011;37:1056-72.
20. Punithakumar K, Hareendranathan AR, McNulty A*, et al*. Multiview 3-D Echocardiography Fusion with Breath-Hold Position Tracking Using an Optical Tracking System. Ultrasound Med Biol. 2016;42:1998-2009.
21. Szmigielski C, Rajpoot K, Grau V*, et al*. Real-time 3D fusion echocardiography. J Am Coll Cardiol Img. 2010;3:682-90.

22. Augustine D, Yaqub M, Szmigielski C*, et al*. "3D fusion" echocardiography improves 3D left ventricular assessment: comparison with 2D contrast echocardiography. Echocardiography. 2015;32:302-9.
23. Li PC, O'Donnell M. Elevational spatial compounding. Ultrason Imaging. 1994;16:176-89.
24. Perperidis A, McDicken N, MacGillivray T, Anderson T. Elevational spatial compounding for enhancing image quality in echocardiography. Ultrasound. 2016;24:74-85.
25. Peressutti D, Gomez A, Penney GP, King AP. Registration of multi-view echocardiography sequences using a subspace error metric. IEEE Trans Biomed Eng. 2017;64:352-61.
26. Mulder HW, van Stralen M, van der Zwaan, Heleen B, Leung KYE, Bosch JG, Pluim JPW. Multiframe registration of real-time three-dimensional echocardiography time series. J Med Imaging. 2014;1:8.
27. Edelman S. Interaction of Sound and Media.Understanding Ultrasound Physics. 4th ed. Woodlands, Texas: E.S.P. Ultrasound, 2012. 75-106.
28. Perperidis A, Cusack D, White A, McDicken N, MacGillivray T, Anderson T. Temporal compounding: a novel implementation and its impact on quality and diagnostic value in echocardiography. Ultrasound Med Biol. 2015;41:1749-65.
29. Amorim JC, Dos Reis, Maria do Carmo, de Carvalho, Joao Luiz Azevedo, da Rocha AF, Camapum JF. Improved segmentation of echocardiographic images using fusion of images from different cardiac cycles. Conf Proc IEEE Eng Med Biol Soc. 2009;2009:511-4.
30. Shahgaldi K, Manouras A, Abrahamsson A, Gudmundsson P, Brodin L, Winter R. Three-dimensional echocardiography using single-heartbeat modality decreases variability in measuring left ventricular volumes and function in comparison to four-beat technique in atrial fibrillation. Cardiovasc Ultrasound. 2010;8:45.
31. Ye X, Noble JA, Declerck J. 3D Freehand Echocardiography for Automatic Left Ventricle Reconstruction and Analysis Based on Multiple Acoustic Windows. Med Image Comput Comput Assist Interv. 2001;2001:778-85.
32. Shekhar R, Zagrodsky V, Garcia MJ, Thomas JD. Registration of real-time 3-D ultrasound images of the heart for novel 3-D stress echocardiography. IEEE Trans Med Imaging. 2004;23:1141-9.
33. Punithakumar K, Hareendranathan A, Noga M, Boulanger P, Becher H. Apparatus and method for generating a fused scan image of a patient 2017.

34. Bersvendsen J, Toews M, Danudibroto A*, et al*. Robust Spatio-Temporal Registration of 4D Cardiac Ultrasound Sequences. Proc SPIE Int Soc Opt Eng. 2016;9790.
35. Maintz JB, Viergever MA. A survey of medical image registration. Med Image Anal. 1998;2:1-36.
36. Hill DL, Batchelor PG, Holden M, Hawkes DJ. Medical image registration. Phys Med Biol. 2001;46:1.
37. Savi A, Gilardi MC, Rizzo G*, et al*. Spatial registration of echocardiographic and positron emission tomographic heart studies. Eur J Nucl Med. 1995;22:243-7.
38. Weiwei Zhang, J. A. Noble, J. M. Brady. Real time 3-D ultrasound to MR cardiovascular image registration using a phase-based approach. Proc IEEE Int Symp Biomed Imaging. 2006;2006:666-9.
39. Zhang W, Brady JM, Becher H, Noble JA. Spatio-temporal (2D+T) non-rigid registration of real-time 3D echocardiography and cardiovascular MR image sequences. Phys Med Biol. 2011;56:1341-60.
40. P. Soler, O. Gerard, P. Allain, E. Saloux, E. Angelini, I. Bloch. Comparison of fusion techniques for 3D+T echocardiography acquisitions from different acoustic windows. Comput Cardiol. 2005;32:141-4.
41. Punithakumar K, Hareendranathan AR, Paakkanen R*, et al*. Multiview echocardiography fusion using an electromagnetic tracking system. Conf Proc IEEE Eng Med Biol Soc. 2016:1078-81.
42. Punithakumar K, Wood PW, Biamonte M, Noga M, Boulanger P, Becher H. Cardiac ultrasound multiview fusion using a multicamera tracking system. IEEE EMBS Int Conf Biomed Health Inform. 2014:318-21.
43. Mulder HW, van Stralen M, Ren B*, et al*. Atlas-Based Mosaicing of Left Atrial 3-D Transesophageal Echocardiography Images. Ultrasound Med Biol. 2017;43:765-74.
44. Chu Y, Yang J, Ma S*, et al*. Registration and fusion quantification of augmented reality based nasal endoscopic surgery. Med Image Anal. 2017;42:241-56.
45. Marinetto E, Victores JG, Garcia-Sevilla M*, et al*. Technical Note: Mobile accelerator guidance using an optical tracker during docking in IOERT procedures. Med Phys. 2017;44:5061-9.
46. Koivukangas T, Katisko JP, Koivukangas JP. Technical accuracy of optical and the electromagnetic tracking systems. Springerplus. 2013;2:90.

47. Nijkamp J, Schermers B, Schmitz S*, et al*. Comparing position and orientation accuracy of different electromagnetic sensors for tracking during interventions. Int J Comput Assist Radiol Surg. 2016;11:1487-98.
48. Badano L, Lang RM, Zamorano JL. Textbook of real-time three dimensional echocardiography. 1st Edition. ed. London: Springer Verlag, 201112.
49. Esposito M, Busam B, Hennersperger C, Rackerseder J, Navab N, Frisch B. Multimodal US–gamma imaging using collaborative robotics for cancer staging biopsies. Int J Comput Assist Radiol Surg. 2016;11:1561-71.
50. Franz AM, Haidegger T, Birkfellner W, Cleary K, Peters TM, Maier-Hein L. Electromagnetic Tracking in Medicine-A Review of Technology, Validation, and Applications. IEEE Trans Med Imag. 2014;33:1702-25.
51. Knight DS, Schwaiger JP, Krupickova S, Davar J, Muthurangu V, Coghlan JG. Accuracy and Test-Retest Reproducibility of Two-Dimensional Knowledge-Based Volumetric Reconstruction of the Right Ventricle in Pulmonary Hypertension. J Am Soc Echocardiogr. 2015;28:989-98.
52. Gao G, Reddy K, Ma Y, Rhode K. Real-time compounding of three-dimensional transesophageal echocardiographic volumes: The phantom study. Paper presented at:31st annual international conference of the IEEE EMBS; Sep 3-6, 2009.
53. Lanzer P, Barta C, Botvinick EH, Wiesendanger HU, Modin G, Higgins CB. ECG-synchronized cardiac MR imaging: method and evaluation. Radiology. 1985;155:681-6.
54. Verschakelen JA, Demedts MG. Normal thoracoabdominal motions. Influence of sex, age, posture, and breath size. Am J Respir Crit Care Med. 1995;151:399-405.
55. Atkinson D, Burcher M, Declerck J, Noble JA. Respiratory motion compensation for 3-D freehand echocardiography. Ultrasound Med Biol. 2001;27:1615-20.
56. Martinez-Moller A, Zikic D, Botnar RM*, et al*. Dual cardiac-respiratory gated PET: implementation and results from a feasibility study. Eur J Nucl Med Mol Imaging. 2007;34:1447-54.
57. Santelli C, Nezafat R, Goddu B*, et al*. Respiratory bellows revisited for motion compensation: preliminary experience for cardiovascular MR. Magn Reson Med. 2011;65:1097-102.
58. Pan T, Lee T, Rietzel E, Chen GTY. 4D-CT imaging of a volume influenced by respiratory motion on multi-slice CT. Med Phys. 2004;31:333-40.

59. Miles B, Ayed IB, Law MWK, Garvin G, Fenster A, Shuo Li. Spine Image Fusion Via Graph Cuts. IEEE Trans Biomed Eng. 2013;60:1841-50.
60. Gooding MJ, Rajpoot K, Mitchell S, Chamberlain P, Kennedy SH, Noble JA. Investigation into the fusion of multiple 4-D fetal echocardiography images to improve image quality. Ultrasound Med Biol. 2010;36:957-66.

61. Rajpoot K, Noble JA, Grau V, Szmigielski C, Becher H. Multiview RT3D echocardiography image fusion. Paper presented at: Functional Imaging and Modeling of the Heart: 5th International Conference, FIMH 2009, Nice, France, June 3-5, 2009.
62. Yao C, Simpson JM, Schaeffter T, Penney GP. Multi-view 3D echocardiography compounding based on feature consistency. Phys Med Biol. 2011;56:6109-28.
63. Ren B, Mulder HW, Haak A*, et al*. A transoesophageal echocardiographic image acquisition protocol for wide-view fusion of three-dimensional datasets to support atrial fibrillation catheter ablation. J Interv Card Electrophysiol. 2013;37:21-6.
64. Piella G, De Craene M, Butakoff C*, et al*. Multiview diffeomorphic registration: application to motion and strain estimation from 3D echocardiography. Med Image Anal. 2013;17:348-64.
65. Carminati MC, Piazzese C, Weinert L*, et al*. Reconstruction of the descending thoracic aorta by multiview compounding of 3-D transesophageal echocardiographic aortic data sets for improved examination and quantification of atheroma burden. Ultrasound Med Biol. 2015;41:1263-76.

2. Chapter II:

1. Lang RM, Badano LP, Mor-Avi V*, et al*. Recommendations for cardiac chamber quantification by echocardiography in adults: an update from the American Society of Echocardiography and the European Association of Cardiovascular Imaging. J Am Soc Echocardiogr. 2015;28:39.e14.
2. Grau V, Szmigielski C, Becher H, Noble JA. Combining apical and parasternal views to improve motion estimation in real-time 3D echocardiographic sequences. Proc IEEE Int Symp Biomed Imaging. 2008:516-9.

3. Grau V, Becher H, Noble JA. Registration of multiview real-time 3-D echocardiographic sequences. IEEE Trans Med Imaging. 2007;26:1154-65.
4. Achenbach S, Friedrich MG, Nagel E*, et al*. CV imaging: what was new in 2012? J Am Coll Cardiol Img. 2013;6:714-34.
5. P. Soler, O. Gerard, P. Allain, E. Saloux, E. Angelini, I. Bloch. Comparison of fusion techniques for 3D+T echocardiography acquisitions from different acoustic windows. Comput Cardiol. 2005;32:141-4.
6. Rajpoot K, Noble JA, Grau V, Szmigielski C, Becher H. Multiview RT3D echocardiography image fusion. Paper presented at: Functional imaging and modeling of the heart: 5th international conference, FIMH 2009, nice, france; June 3-5, 2009.
7. Rajpoot K, Grau V, Noble JA, Szmigielski C, Becher H. Multiview Fusion 3-d Echocardiography: Improving the Information and Quality of Real-Time 3-D Echocardiography. Ultrasound Med Biol. 2011;37:1056-72.
8. Rajpoot K, Grau V, Noble JA, Becher H, Szmigielski C. The evaluation of single-view and multi-view fusion 3D echocardiography using image-driven segmentation and tracking. Med Image Anal. 2011;15:514-28.
9. Gooding MJ, Rajpoot K, Mitchell S, Chamberlain P, Kennedy SH, Noble JA. Investigation into the fusion of multiple 4-D fetal echocardiography images to improve image quality. Ultrasound Med Biol. 2010;36:957-66.
10. Szmigielski C, Rajpoot K, Grau V*, et al*. Real-time 3D fusion echocardiography. J Am Coll Cardiol Img. 2010;3:682-90.
11. Yao C, Simpson JM, Schaeffter T, Penney GP. Multi-view 3D echocardiography compounding based on feature consistency. Phys Med Biol. 2011;56:6109-28.
12. Ren B, Mulder HW, Haak A*, et al*. A transoesophageal echocardiographic image acquisition protocol for wide-view fusion of three-dimensional datasets to support atrial fibrillation catheter ablation. J Interv Card Electrophysiol. 2013;37:21-6.
13. Piella G, De Craene M, Butakoff C*, et al*. Multiview diffeomorphic registration: application to motion and strain estimation from 3D echocardiography. Med Image Anal. 2013;17:348-64.
14. Augustine D, Yaqub M, Szmigielski C*, et al*. "3D fusion" echocardiography improves 3D left ventricular assessment: comparison with 2D contrast echocardiography. Echocardiography. 2015;32:302-9.

15. Carminati MC, Piazzese C, Weinert L*, et al*. Reconstruction of the descending thoracic aorta by multiview compounding of 3-D transesophageal echocardiographic aortic data sets for improved examination and quantification of atheroma burden. Ultrasound Med Biol. 2015;41:1263-76.
16. Punithakumar K, Hareendranathan AR, McNulty A*, et al*. Multiview 3-D Echocardiography Fusion with Breath-Hold Position Tracking Using an Optical Tracking System. Ultrasound Med Biol. 2016;42:1998-2009.
17. Danudibroto A, Bersvendsen J, Gerard O, Mirea O, D'hooge J, Samset E. Spatiotemporal registration of multiple three-dimensional echocardiographic recordings for enhanced field of view imaging. J Med Imaging. 2016;3:037001.
18. Peressutti D, Gomez A, Penney GP, King AP. Registration of multi-view echocardiography sequences using a subspace error metric. IEEE Trans Biomed Eng. 2017;64:352-61.
19. Thomas JD, Rubin DN. Tissue harmonic imaging: Why does it work? J Am Soc Echocardiogr. 1998;11:803-8.
20. Lang RM, Badano LP, Tsang W*, et al*. EAE/ASE recommendations for image acquisition and display using three-dimensional echocardiography. J Am Soc Echocardiogr. 2012;13:1-46.
21. Badano L, Lang RM, Zamorano JL. Textbook of real-time three dimensional echocardiography. 1st Edition. ed. London: Springer Verlag, 201112.
22. Welvaert M, Rosseel Y. On the definition of signal-to-noise ratio and contrast-to-noise ratio for FMRI data. PLoS One. 2013;8:e77089.
23. Joel SE, Caffo BS, van Zijl, Peter C M, Pekar JJ. On the relationship between seed-based and ICA-based measures of functional connectivity. Magn Reson Med. 2011;66:644-57.
24. Chen H, Yao D. Discussion on the choice of separated components in fMRI data analysis by spatial independent component analysis. Magn Reson Imaging. 2004;22:827-33.
25. Shrout PE, Fleiss JL. Intraclass correlations: uses in assessing rater reliability. Psychol Bull. 1979;86:420-8.
26. Fleiss JL, Levin BA, Paik MC. Statistical methods for rates and proportions. 3. ed. Hoboken, NJ: Wiley, 2003.
27. Sheskin DJ. Handbook of parametric and nonparametric statistical procedures. 4. ed. Boca Raton [u.a.]: Chapman & Hall/CRC, 2007.

28. Cicchetti DV. Guidelines, Criteria, and Rules of Thumb for Evaluating Normed and Standardized Assessment Instruments in Psychology. Psychol Assess. 1994;6:284-90.

3. Chapter III:

1. Szmigielski C, Rajpoot K, Grau V*, et al*. Real-time 3D fusion echocardiography. J Am Coll Cardiol Img. 2010;3:682-90.
2. Lanzer P, Barta C, Botvinick EH, Wiesendanger HU, Modin G, Higgins CB. ECG-synchronized cardiac MR imaging: method and evaluation. Radiology. 1985;155:681-6.
3. Atkinson D, Burcher M, Declerck J, Noble JA. Respiratory motion compensation for 3-D freehand echocardiography. Ultrasound Med Biol. 2001;27:1615-20.
4. Martinez-Moller A, Zikic D, Botnar RM*, et al*. Dual cardiac-respiratory gated PET: implementation and results from a feasibility study. Eur J Nucl Med Mol Imaging. 2007;34:1447-54.
5. Pan T, Lee T, Rietzel E, Chen GTY. 4D-CT imaging of a volume influenced by respiratory motion on multi-slice CT. Med Phys. 2004;31:333-40.
6. Verschakelen JA, Demedts MG. Normal thoracoabdominal motions. Influence of sex, age, posture, and breath size. Am J Respir Crit Care Med. 1995;151:399-405.
7. De Groote A, Wantier M, Cheron G, Estenne M, Paiva M. Chest wall motion during tidal breathing. J Appl Physiol. 1997;83:1531-7.
8. de Groote A, Verbandt Y, Paiva M, Mathys P. Measurement of thoracoabdominal asynchrony: importance of sensor sensitivity to cross section deformations. J Appl Physiol. 2000;88:1295-302.
9. Ehman RL, McNamara MT, Pallack M, Hricak H, Higgins CB. Magnetic resonance imaging with respiratory gating: techniques and advantages. Am J Roentgenol. 1984;143:1175-82.
10. Franz AM, Haidegger T, Birkfellner W, Cleary K, Peters TM, Maier-Hein L. Electromagnetic Tracking in Medicine-A Review of Technology, Validation, and Applications. IEEE Trans Med Imag. 2014;33:1702-25.
11. Zhang HK, Cheng A, Bottenus N, Guo X, Trahey GE, Boctor EM. Synthetic tracked aperture ultrasound imaging: design, simulation, and experimental evaluation. J Med Imaging. 2016;3:027001.

12. Bottenus N, Long W, Zhang HK*, et al*. Feasibility of Swept Synthetic Aperture Ultrasound Imaging. IEEE Trans Med Imaging. 2016;35:1676-85.
13. Monfaredi R, Wilson E, Azizi Koutenaei B*, et al*. Robot-assisted ultrasound imaging: overview and development of a parallel telerobotic system. Minim Invasive Ther Allied Technol. 2015;24:54-62.
14. Noble JA, Navab N, Becher H. Ultrasonic image analysis and image-guided interventions. Interface Focus. 2011;1:673-85.
15. Mulder HW, van Stralen M, Ren B*, et al*. Atlas-Based Mosaicing of Left Atrial 3-D Transesophageal Echocardiography Images. Ultrasound Med Biol. 2017;43:765-74.
16. Ren B, Mulder HW, Haak A*, et al*. A transoesophageal echocardiographic image acquisition protocol for wide-view fusion of three-dimensional datasets to support atrial fibrillation catheter ablation. J Interv Card Electrophysiol. 2013;37:21-6.
17. Carminati MC, Piazzese C, Weinert L*, et al*. Reconstruction of the descending thoracic aorta by multiview compounding of 3-D transesophageal echocardiographic aortic data sets for improved examination and quantification of atheroma burden. Ultrasound Med Biol. 2015;41:1263-76.
18. Kalashyan H, Shuaib A, Gibson PH*, et al*. Single sweep three-dimensional carotid ultrasound: Reproducibility in plaque and artery volume measurements. Atherosclerosis. 2014;232:397-402.